NAVAL POSTGRADUATE SCHOOL

MONTEREY, CALIFORNIA

THESIS

PROPAGATION AND PERFORMANCE ANALYSIS FOR A 915 MHZ WIRELESS IR IMAGE TRANSFER SYSTEM

by

Oktay Felekoglu

June 2005

Thesis Advisor: Richard M. Harkins
Co-Advisor : Gamani Karunasiri

Approved for public release; distribution is unlimited

THIS PAGE INTENTIONALLY LEFT BLANK

REPORT DOCUMENTATION PAGE			Form Approved OMB No. 0704-0188
Public reporting burden for this collection of information is estimated to average 1 hour per response, including the time for reviewing instruction, searching existing data sources, gathering and maintaining the data needed, and completing and reviewing the collection of information. Send comments regarding this burden estimate or any other aspect of this collection of information, including suggestions for reducing this burden, to Washington headquarters Services, Directorate for Information Operations and Reports, 1215 Jefferson Davis Highway, Suite 1204, Arlington, VA 22202-4302, and to the Office of Management and Budget, Paperwork Reduction Project (0704-0188) Washington DC 20503.			
1. AGENCY USE ONLY ***(Leave blank)***	**2. REPORT DATE** June 2005	**3. REPORT TYPE AND DATES COVERED** Master's Thesis	
4. TITLE AND SUBTITLE: Propagation and Performance Analysis for a 915 MHz Wireless IR Image Transfer System			**5. FUNDING NUMBERS**
6. AUTHOR(S) OKTAY FELEKOGLU			
7. PERFORMING ORGANIZATION NAME(S) AND ADDRESS(ES) Naval Postgraduate School Monterey, CA 93943-5000			**8. PERFORMING ORGANIZATION REPORT NUMBER**
9. SPONSORING /MONITORING AGENCY NAME(S) AND ADDRESS(ES) N/A			**10. SPONSORING/MONITORING AGENCY REPORT NUMBER**
11. SUPPLEMENTARY NOTES The views expressed in this thesis are those of the author and do not reflect the official policy or position of the Department of Defense or the U.S. Government.			
12a. DISTRIBUTION / AVAILABILITY STATEMENT Approved for public release; distribution is unlimited			**12b. DISTRIBUTION CODE**

13. ABSTRACT

A 915 MHz wireless IR image transfer system, comprised of an IR-160 Thermal Camera and MDS iNet 900 transceivers, was assessed for image transfer capabilities in different environments. Image transfer through natural and artificial obstructions, the capability of transferring images under urban environments, and an exploration of interference issues associated with RF communication links were investigated in detail. Concrete, wood, various construction materials, and building walls were examined to assess indoor propagation capabilities. Data transmission through random trees, buildings, foliage under various atmospheric conditions is also evaluated for outdoor system capabilities. A maximum free space range for acceptable IR image transferring is determined as 23 miles for line of sight (LOS). Non line of sight (NLOS) urban environment measurements revealed that urban path loss (15-60 dBm) is highly dependent on antenna orientation and obstruction geometry rather than the T-R separation distance.

14. SUBJECT TERMS EM Propagation, Path Loss, Wireless Image Transfer, IR Imaging, Remote Sensing			**15. NUMBER OF PAGES** 97
			16. PRICE CODE
17. SECURITY CLASSIFICATION OF REPORT Unclassified	**18. SECURITY CLASSIFICATION OF THIS PAGE** Unclassified	**19. SECURITY CLASSIFICATION OF ABSTRACT** Unclassified	**20. LIMITATION OF ABSTRACT** UL

NSN 7540-01-280-5500 Standard Form 298 (Rev. 2-89)
Prescribed by ANSI Std. 239-18

THIS PAGE INTENTIONALLY LEFT BLANK

Approved for public release; distribution is unlimited

PROPAGATION AND PERFORMANCE ANALYSIS FOR A 915 MHZ WIRELESS IR IMAGE TRANSFER SYSTEM

Oktay Felekoglu
First Lieutenant, Turkish Army
B.S., Turkish Army Academy, 2000

Submitted in partial fulfillment of the
requirements for the degree of

MASTER OF SCIENCE IN APPLIED PHYSICS

from the

NAVAL POSTGRADUATE SCHOOL
June 2005

Author: Oktay Felekoglu

Approved by: Richard M. Harkins
Thesis Advisor

Gamani Karunasiri
Co-Advisor

James H. Luscombe
Chairman, Department of Physics

THIS PAGE INTENTIONALLY LEFT BLANK

ABSTRACT

A 915 MHz wireless IR image transfer system, comprised of an IR-160 Thermal Camera and MDS iNet 900 transceivers, was assessed for image transfer capabilities in different environments. Image transfer through natural and artificial obstructions, the capability of transferring images under urban environments, and an exploration of interference issues associated with RF communication links were investigated in detail. Concrete, wood, various construction materials, and building walls were examined to assess indoor propagation capabilities. Data transmission through random trees, buildings, foliage under various atmospheric conditions is also evaluated for outdoor system capabilities. A maximum free space range for acceptable IR image transferring is determined as 23 miles for line of sight (LOS). Non line of sight (NLOS) urban environment measurements revealed that urban path loss (15-60 dBm) is highly dependent on antenna orientation and obstruction geometry rather than the T-R separation distance.

THIS PAGE INTENTIONALLY LEFT BLANK

TABLE OF CONTENTS

LIST OF FIGURES

LIST OF TABLES

THIS PAGE INTENTIONALLY LEFT BLANK

LIST OF ABBREVIATIONS AND SYMBOLS

$\vec{E}$	=	Electric field intensity (V/m)
$\vec{B}$	=	Magnetic field intensity (A/m)
ρ	=	Volume charge density
$\vec{J}$	=	Volume current density
ε_0	=	8.854×10^{-12} (F/m), Permittivity of free space
μ_0	=	1.257×10^{-6} (H/m), Permeability of free space
$\vec{S}$	=	Poynting vector or energy flux density
P_t	=	Transmitted power
P_r	=	Received power as a function of distance
G_t	=	Transmitter antenna gain
G_r	=	Receiver antenna gain
r	=	Distance between transmitter and receiver
χ	=	System loss factor
A_e	=	Effective antenna aperture
Z_0	=	Impedance of free space
E_{fs}	=	Free space E-field
P	=	Power flux density
L_{fs}	=	Free space loss
r_f	=	Fraunhofer region beginning distance
θ_c	=	Brewster angle
L_{diff}	=	Diffraction loss
D	=	Antenna directivity
SWR	=	Standing wave ratio
VSWR	=	Voltage standing wave ratio
RSSI	=	Received signal strength indicator
dB	=	Decibels
IR	=	Infrared

T	=	Transmitter
R	=	Receiver
EIRP	=	Effective isotropic radiator power
r_{Fn}	=	n^{th} Fresnel zone radius
AFT	=	Average file transfer time
FS	=	File size
$\hat{p}$	=	Successful file transfer probability
Λ’	=	Voltage reflection coefficient
γ	=	Antenna efficiency
L_{median}	=	Median loss (Hata model)
ξ	=	Urban correction factor (Hata Model)
σ	=	Standard deviation
$\tilde{\sigma}$	=	Conductivity
ρ_s	=	Scattering loss factor
h_T	=	Transmitter antenna height
h_R	=	Receiver antenna height
LOS	=	Line of sight
NLOS	=	Non-line of sight
ISM	=	Industrial, scientific, medical
UDP	=	User datagram protocol
TCP/IP	=	Transmission control protocol/Internet protocol
$\Lambda_{\parallel}$	=	Fresnel reflection coefficient for parallel polarized E-field at the reflection surface
$\Lambda_{\perp}$	=	Fresnel reflection coefficient for vertical polarized E-filed at the reflection surface

ACKNOWLEDGEMENTS

I would like to express my sincere gratitude to my thesis advisor, Professor Richard Harkins, for his guidance and patience during this thesis study.

I would also like to thank Professor Gamani Karunasiri for his assistance and encouragement in this thesis.

It was my friends' unending support that eased all the difficulties.

And no need to mention about my beloved family without whose precious presence any success would be meaningless.

THIS PAGE INTENTIONALLY LEFT BLANK

I. INTRODUCTION

A. BACKGROUND

The urban environment has become a significant element in the modern combat field. The ambiguity of the urban environment, along with an undetectable enemy presence, seems to be the major cause of losses in low intensity conflicts. Enhanced surveillance is the key solution decreasing the number of casualties in an urban-combat field. Autonomous remote IR sensing systems can be employed for surveillance and target detection purposes to minimize human involvement in the process. With this goal in mind, a wireless IR image transfer system comprised of an IR camera, two transceivers and various antennas was previously built to be finally deployed on the Naval Postgraduate School's (NPS) autonomous ground vehicle. Details of this previous work are presented in "Wireless IR Image Transfer System for an Autonomous Vehicle." [1]

Establishing a wireless communication link between the sensing unit(s) and the control unit(s) is required in order to achieve an autonomous remote sensing ability. The performance and efficiency of the whole sensing system will be directly dependent on how accurately the objective data are transferred between the end units. At this point, understanding the nature of electromagnetic waves and their propagation mechanisms through various media becomes vital for determining the performance assessment of these kinds of remote sensing systems.

B. ELECTROMAGNETIC WAVES

The expression "*electromagnetic wave*" is used to describe the intrinsic phenomena of propagation of electric and magnetic fields through free space or various media with specific velocities. In order to utilize the high speed of this peculiar wave motion, information is impressed on the electromagnetic waves by modifying amplitude, phase or frequency with special techniques and is sent through the separating media. Electromagnetic wave motion has its own characteristics buried in the Maxwell's Equations.

1. Maxwell's Equations

It has long been known that an electric current produces a magnetic field and that a changing magnetic field produces an electric field. This subtle relationship was gracefully put together by Maxwell in the following concise form, known as Maxwell's Equations in general [4, 5]

$$\vec{\nabla} \bullet \vec{E} = \frac{\rho}{\varepsilon_0} \tag{1.1}$$

$$\vec{\nabla} \times \vec{E} = -\frac{\partial \vec{B}}{\partial t} \tag{1.2}$$

$$\vec{\nabla} \times \vec{B} = 0 \tag{1.3}$$

$$\vec{\nabla} \times \vec{B} = \mu_0 \vec{J} + \mu_0 \varepsilon_0 \frac{\partial \vec{E}}{\partial t} \tag{1.4}$$

Equation 1.2 simply states that a magnetic field changing with time gives rise to an electric field. Similarly, equation 1.4 shows that time-dependent variations in an electric field produce a magnetic field. Notice that for the case of electromagnetic waves in matter, the equations above are expressed in slightly different forms inducing the same results. [4] Imagine two stationary point charges. On the line path of the smallest distance connecting these two charges there will be an attractive or repellant force depending on the sign of the charges. The magnitude and direction of this force per unit charge is defined as an electric field. When the charges move there will be a consequent change in electric field and this change will create a magnetic field and a magnetic flux density. [5] The continuously varying electric and magnetic fields will produce an electromagnetic wave which will propagate at a speed given by $v = \frac{1}{\sqrt{\mu\varepsilon}}$ (m/s).Where μ and ε are respectively, permeability and permittivity of the propagation medium. The speed of an

electromagnetic wave in a linear homogenous media is related to speed of light as $v = \frac{c}{n}$, here *n* is the index of refraction of the material and is given by $n \equiv \sqrt{\frac{\varepsilon\mu}{\varepsilon_0\mu_0}}$.

2. Impedance of Free Space and Transmission Media

The ratio of the magnitudes of electric and magnetic fields results in a specific resistance called impedance. For free space, impedance is given by $z_0 = \sqrt{\frac{\mu_0}{\varepsilon_0}} \approx 120\pi\Omega = 377\Omega$. Where $\mu_0 = 4\pi \times 10^{-7}$ (Vs/Am) is the permeability of free space and $\varepsilon_0 = (10^{-9}/36\pi)$ (As/Vm) is the permittivity. In a similar fashion, impedance of any transmission medium is obtained by replacing the constants μ_0 and ε_0 with $\mu = \mu_0\mu_r$ (H/m) and $\varepsilon = \varepsilon_0\varepsilon_r$ (F/m). [4]

3. Poynting Vector and Power in EM Waves

Electromagnetic fields carry a certain amount of energy. The amount of the total energy (W_T) stored in electromagnetic fields is equal to

$$W_T = \frac{1}{2}\int (\varepsilon_0 E^2 + \frac{1}{\mu_0} B^2) d\vartheta \qquad (1.5)$$

Here $d\vartheta$ is the volume element. [4]

The Poynting vector defines the energy carried by electromagnetic fields, per unit time per unit area, and is given by [4]

$$\vec{S} = \frac{1}{\mu_0}(\vec{E} \times \vec{B}) \qquad (1.6)$$

The average power per unit area transported by an electromagnetic wave is called the intensity which is equal to [4]

$$I \equiv \frac{1}{2} v \varepsilon E_0^{\,2} \qquad (1.7)$$

4. Polarization

The polarization of an electromagnetic wave is determined with the orientation of the electric field relative to the earth. EM is said to be vertically polarized if the E-field is perpendicular to the earth, and vice versa for horizontal polarization (Figure 1). When the E and B-fields rotate around the propagation axis due to the phase difference between them, a third form of polarization occurs. The third form of polarization is called elliptical polarization. Polarization has direct effects on EM wave matter interaction. [4, 5]

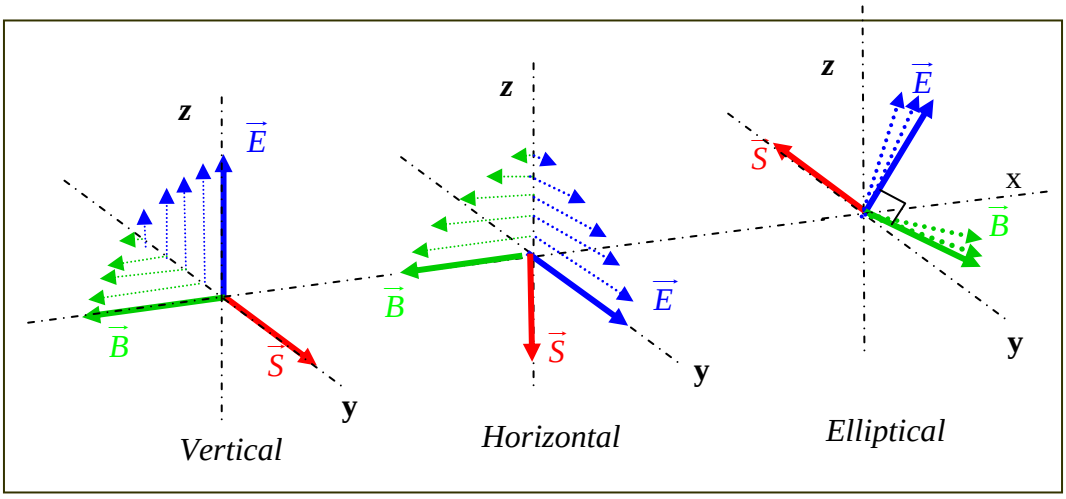

Figure 1. Wave polarizations.

C. ELECTROMAGNETIC WAVE PROPAGATION

In urban environments, the paths along which EM waves travel can vary both in length and in route due to multiple reflections from various objects. Multi-path fading occurs at specific points as a result of interactions between these waves. A certain amount of attenuation is unavoidable when EM waves pass through different media. All these effects cause a difference in transmitted and received powers; this total difference is named *path loss*.

1. Free Space Propagation

In free space, the emitted power per unit area (W/m^2) or the magnitude of Poynting vector, gives us the power flux density p as

$$p = \frac{P_t G_t}{4\pi r^2} = \frac{E_{fs}{}^2}{z_0} = \frac{|E|^2}{377\Omega} \quad (W/m^2) \tag{1.8}$$

where P_t is the transmitted power, G_t is the gain of transmitter antenna, E_{fs} is the electric field in free space, r is the distance between transmitter and receiver and z_0 is the impedance.

When there is no obstruction between the transmitter and the receiver and when they are in line-of-sight; an approximate free space propagation model (Friis Equation) can be used to express received power in terms of transmitted power, wave length, antenna gains (G_t, G_r), and distance (r)

$$P_r = \frac{P_t G_t G_r}{\chi}\left(\frac{\lambda}{4\pi r}\right)^2 = \left(\frac{P_t G_t}{4\pi r^2}\right)\frac{A_e}{\chi} = p\frac{A_e}{\chi} \tag{1.9}$$

P_r is the received power and A_e is the effective antenna aperture.

Effective antenna aperture A_e is a function of gain (G) and wave length

$$A_e = \frac{G\lambda^2}{4\pi} \tag{1.10}$$

The system loss factor (i.e. losses caused by system components but not by the attenuation due to propagation) is given by χ. [2] For the ideal case, the value of the system loss factor is χ =1. A radiating source sending out EM waves in all directions with equal field strengths and 100% efficiency is called an isotropic radiator and represents the ideal case. *Effective isotropic radiated power* (EIRP=$P_t G_t$) is the maximum transmitted power in direction of maximum antenna gain. However, it is more practical to use effective radiated power (*ERP*) instead of *EIRP* by replacing the ideal isotropic radiator with a half-wave dipole antenna. [2] In a free space model path loss which is the difference (in dB) between the effective P_t and P_r is defined in [2] as

$$L_{fs}(dB) = 10 \log \frac{P_t}{P_r} = -10 \log[G_t G_r (\frac{\lambda}{4\pi r})^2] \quad (1.11)$$

The far field, *the Fraunhofer Region,* begins after distance $d_f = \frac{2L^2}{\lambda}$ where L is the maximum dimension of the antenna (Figure 2). For d_f to be considered in far field $d_f >> L$ and $d_f >> \lambda$ are also required conditions. *Friis free space propagation formula* is only applicable for r (transmitter and receiver separation) values which are in far field according to the transmitting source. [2, 5]

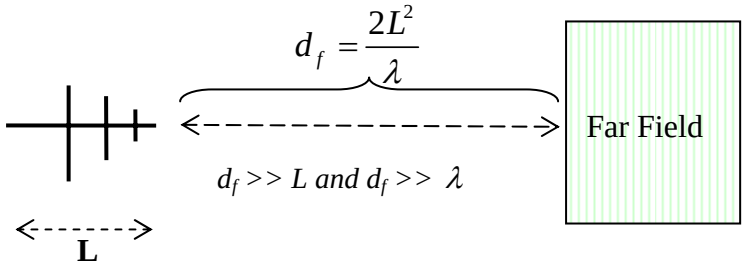

Figure 2. Far field and maximum dimension of antenna.

Free space path loss (L_{fs}) in decibels as a function of frequency (f) and distance (r) is equal to [2]

$$L_{fs} = 32.45 + 20 \log f(MHz) + 20 \log r\ (km) \quad (1.12)$$

The LOS path between transmitter and receiver is accepted to be clear of obstacles when the first Fresnel zone is free of obstacles by 0.6 r_{F1} (Figure 3). [11] In this relationship r_{F1} is the radius of first Fresnel zone and is given by

$$r_{F1} = \sqrt{\frac{\lambda d_t d_r}{(d_t + d_r)}} \quad (1.13)$$

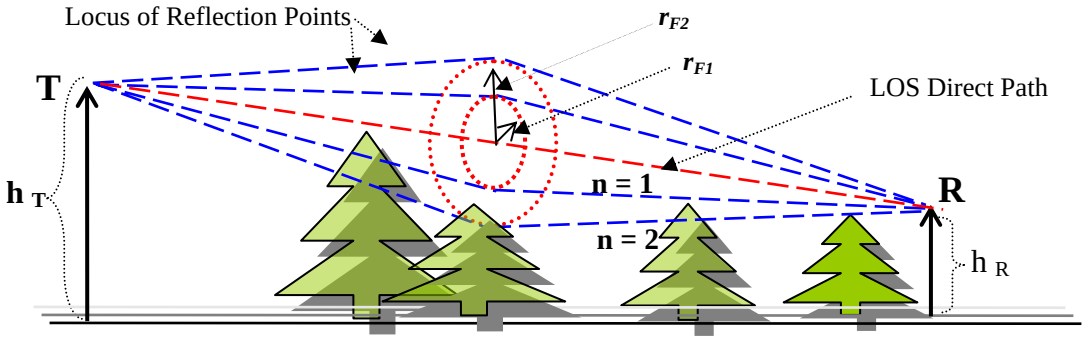

Figure 3. Fresnel zones. In the diagram first and second Fresnel zones (r_{F1} and r_{F2}) are obstructed by the trees.

2. Propagation Mechanisms

There are three main mechanisms concerning electromagnetic wave propagation: reflection, diffraction, and scattering.

a. Reflection

A sudden change in the electrical properties of the medium in which an electromagnetic wave is propagating causes partial reflection of the wave, while the remaining part is transmitted with a certain amount of absorption depending on the material's properties, frequency, polarization, and angle of incidence (Figure 4). In the case of reflection from a perfect dielectric, no absorption occurs. [2, 5] A second medium of a perfect conductor on the path of propagation does not allow EM waves to penetrate and all the incident energy is reflected back without any transmission. [4]

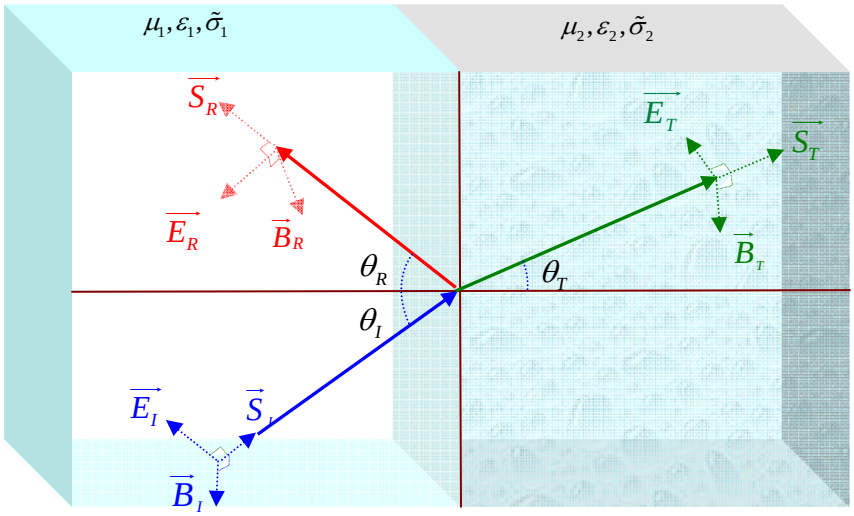

Figure 4. Reflection and transmission of a linearly polarized electromagnetic wave propagating in two different media.

The reflection coefficient Λ is equal to the ratio of E_r to E_i. In cases of parallel and perpendicular E-field polarization at the reflection surface, Λ is given by

$$\Lambda_{\parallel} = \frac{z_2 \sin\theta_T - z_1 \sin\theta_I}{z_2 \sin\theta_T + z_1 \sin\theta_I} \tag{1.14}$$

$$\Lambda_{\perp} = \frac{z_2 \sin\theta_I - z_1 \sin\theta_T}{z_2 \sin\theta_I + z_1 \sin\theta_T} \tag{1.15}$$

At some critical angle θ_C, $\Lambda_{\parallel}$ becomes zero (i.e., no reflection). This angle is called the Brewster angle and is equal to

$$\theta_C = \sin^{-1}\left(\sqrt{\frac{\varepsilon_1}{\varepsilon_1 + \varepsilon_2}}\right) \tag{1.16}$$

If the reflecting surface is a perfect conductor, reflection coefficients simply reduce; $\Lambda_{\parallel}$=1 and $\Lambda_{\perp} = -1$, dependence on the angle of incidence disappears.

b. Diffraction

When the path of an EM wave is partially blocked by an object, a considerable portion of the obstructed wave continues its propagation in the shadowed region (Figure 5). As explained in Huygen's principle, secondary waves occur behind the object. These waves carry the information inherited from the primary waves to the shadow. This peculiar wave behavior is called diffraction and it is highly dependent on obstruction geometry. In practical usage of a wireless link, diffraction may occur due to obstructions like buildings, cars, hills, etc. Given the complexity of the obstruction geometry, an exact mathematical formulation of the effects of diffraction in urban wireless communication links is extremely difficult. Approximating the complicated obstruction structure to a knife edge or wedge model is a commonly used technique for mathematical simplification (Figure 5).

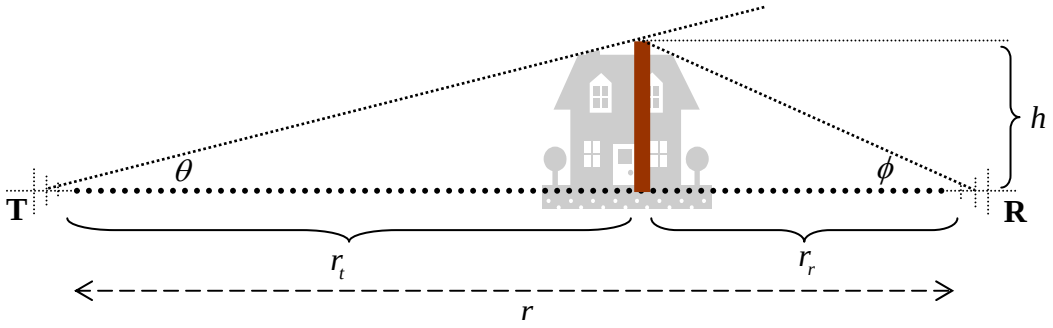

Figure 5. Knife edge approximation geometry for diffraction.

The following equations are derived from the equations that appear in [5] and [6] to determine the approximate diffraction loss (L_{diff}) over a single knife edge model (Figure 5) in dB

$$L_{diff} = 6.02 + 23.24\sqrt{\kappa} + 11\kappa, \qquad \kappa < 0 \tag{1.17}$$

$$L_{diff} = 6.02 + 23.52\sqrt{\kappa} - 8.47\kappa, \qquad 0 < \kappa \le 2.4 \tag{1.18}$$

$$L_{diff} = 21.19 + 10\log(\kappa), \qquad \kappa > 2.4 \tag{1.19}$$

where κ is a parameter derived from the geometry of diffraction as depicted in Figure 5, and is given by

$$\kappa = f(MHz) r \tan\theta \tan\phi \tag{1.20}$$

Since $\tan\phi = \frac{h}{r_r}$ and $\tan\theta = \frac{h}{r_t}$, where h is the height of the obstacle and θ and ϕ are the angles as shown on Figure 5, then κ can be written as

$$\kappa = h^2 \frac{f(MHz) r}{r_t r_r} \tag{1.21}$$

As the number of obstructions increases, the total diffraction loss may be estimated by summing the losses from each individual edge. For every diffracting edge κ should be calculated separately. The preceding obstacle is treated as the transmitter for its successor. [5] This approach is known as the *Epstein-Peterson* method (Figure 6). [7] Total diffraction loss from multiple obstacles is then given by

$$L_{Total\ diff} = \sum_{i}^{n} L_{i\ diff} \tag{1.22}$$

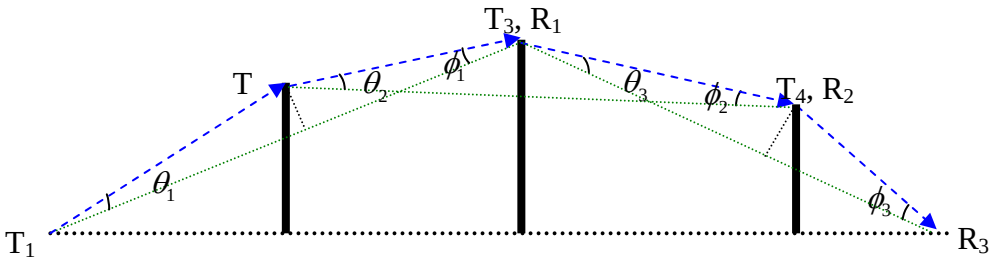

Figure 6. Epstein-Peterson method geometry for diffraction on multiple knife edge obstacles. [After Ref. 5]

Since the parameter κ depends directly on the frequency of the system and the angles θ and ϕ (Figures 5 and 6) as defined in equation 1.20, an increase in these angles or in frequency will augment the diffraction loss. By locating the transmitter and the receiver away from the obstacles, the angles θ and ϕ can be decreased, and thus the diffraction loss (L_{diff}) also decreases.

c. Scattering

The reflection of energy from rough surfaces on which specular reflection is not possible gives rise to scattering. The strong interdependence between angle of incidence and angle of reflection disappears when the surface is rough or has small dimensions compared to the incident wavelength. The diminishing effect of scattering in a reflected field is accounted for by multiplying the reflection coefficients with a probabilistic function, ρ_s, scattering loss factor [2]

$$\rho_s = e^{[-8(\frac{\pi\sigma_h \sin\theta_I}{\lambda})^2]} I_0[8(\frac{\pi\sigma_h \sin\theta_I}{\lambda})^2] \tag{1.23}$$

where I_0 is the Bessel function of the first kind and zero order and σ_h is the standard deviation of the mean surface height. Then the corrected reflection coefficient for scattering surfaces ($\Lambda_{scattered}$) will be equal to [2]

$$\Lambda_{scattered} = \rho_s \Lambda \tag{1.24}$$

THIS PAGE INTENTIONALLY LEFT BLANK

II. WIRELESS IR IMAGE TRANSFER SYSTEM COMPONENTS

The wireless IR image transfer system is comprised of two transceivers (MDS iNET 900) operating at a center frequency of 915 MHZ, an IR thermal camera, two Yagi antennas, a computer terminal, and power supply units. As explained in [1], a point-to-point user datagram protocol (UDP) wireless data link is formed by setting one of the transceivers as the access point (control unit) while the other one is set to work as the remote unit (see Figure 7).

The infrared imaging camera is attached to the remote unit through an RS 232 serial data link. Images captured by the camera are sent to the RS 232 serial port of the remote unit. The image file, which is in the form of serial data, is turned into UDP packets at the remote unit, and transmitted with the help of directional Yagi antenna attached to the transceiver. The transmitted data is received by the receiver antenna of the access point. The data in the UDP format is again turned into serial data form at the access point. The transferred image file is viewed by a computer connected to the access point. This communication link can be operated in the reverse direction in the same fashion.

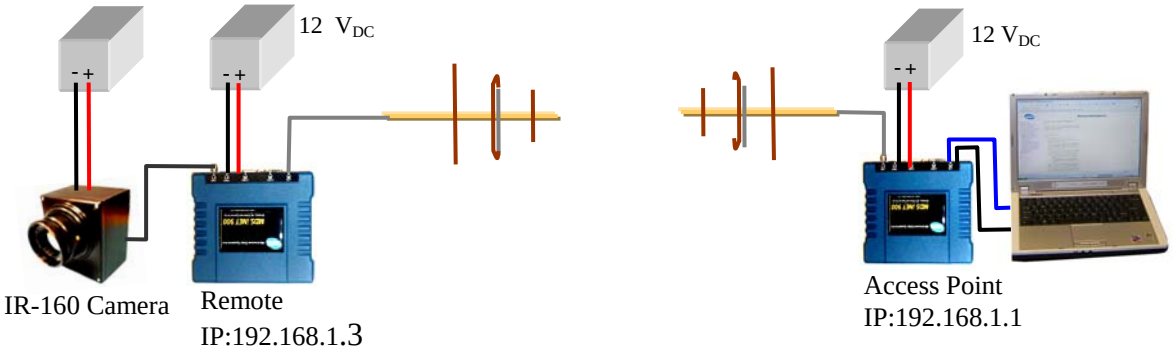

Figure 7. Point-to-Point wireless IR image transfer system components.

A. IR-160 CAMERA

The IR-160 infrared camera is the data source for our remote sensing unit. The camera is sensitive to the long wave infrared band with a temperature resolution under

0.08 ^{0} C, and is therefore capable of providing images under complete darkness. IR-160 utilizes uncooled microbolometer technology. By eliminating the external cooling process the camera minimizes power consumption and enhances the possibility of versatile military employment. It can be operated between 0 and 50^{o} C; quite broad range for military deployment. [1, 8]

The main output of the camera is 160 x 120 pixel NTSC video signal. It also provides portable grayscale bitmap files through the RS-232 serial communication link (Figure 8).

Commands can be sent through the serial port for set up and control purposes. [1, 8] Detailed technical specifications and a table of computer commands are provided in Appendices A and B.

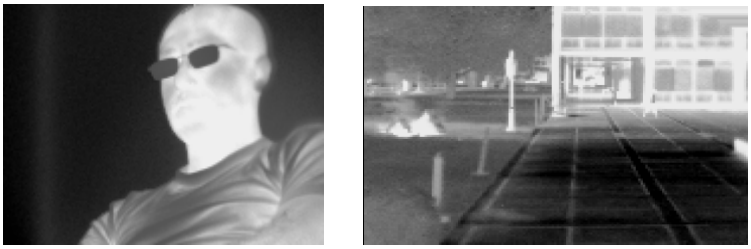

Figure 8. Sample images from IR-160 camera.

B. MDS INET 900 (902-928 MHZ) TRANSCEIVERS

The infrared image transfer mechanism which was first built by Ata as explained in [1], utilized MDS iNET 900 transceivers (Figure 9) as the main data transfer apparatus. The transceivers are also the subjects of experiments in this study. They operate at frequencies between 902-928 MHz and provide a maximum RF power output of +30 dBm (1 Watt). They use ethernet RJ-45 and RS-232 serial interfaces for communication. The transceivers require 10-30 Volts DC to operate. [9]

Network, radio, performance, and other set up parameters can be changed by using the built-in management system which can be reached by COM1 and ethernet ports. [9] An embedded HTTP web-server is also available. For our experiment, one

transceiver is set as the access point and the other is set as the remote unit. The access point and remote unit are assigned the IP addresses 192.168.1.1 and 192.168.1.3 respectively.

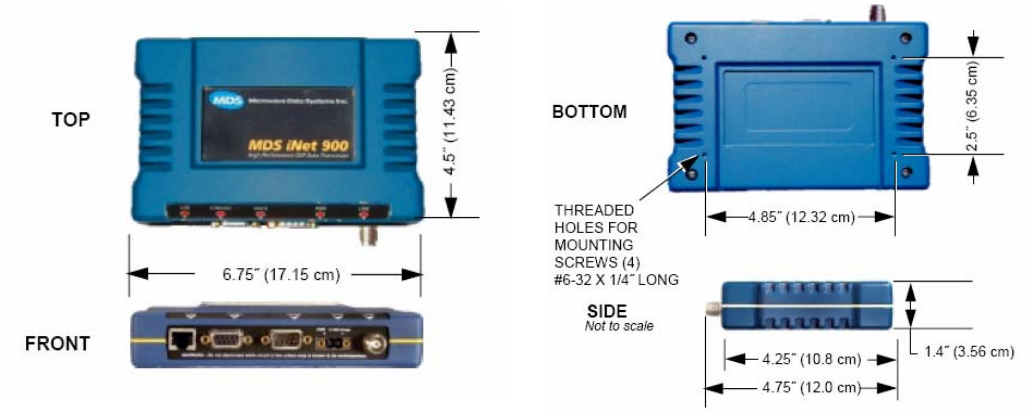

Figure 9. Transceiver dimensions and connection ports. [From Ref. 9]

The approximate boot time for the access point is determined to be 30 seconds, and the time required to associate with the remote is found as 25 seconds. See Appendix C for more detailed design specifications.

C. YAGI ANTENNA

1. Antenna Design

Two directional three-element folded dipole antennas (Figure 10) are used at both ends of the data link. [1, 17] The directionality of the antennas, providing 6 dB gain, is intended to increase the system efficiency with proper antenna orientation. See Appendix D for detailed design specifications.

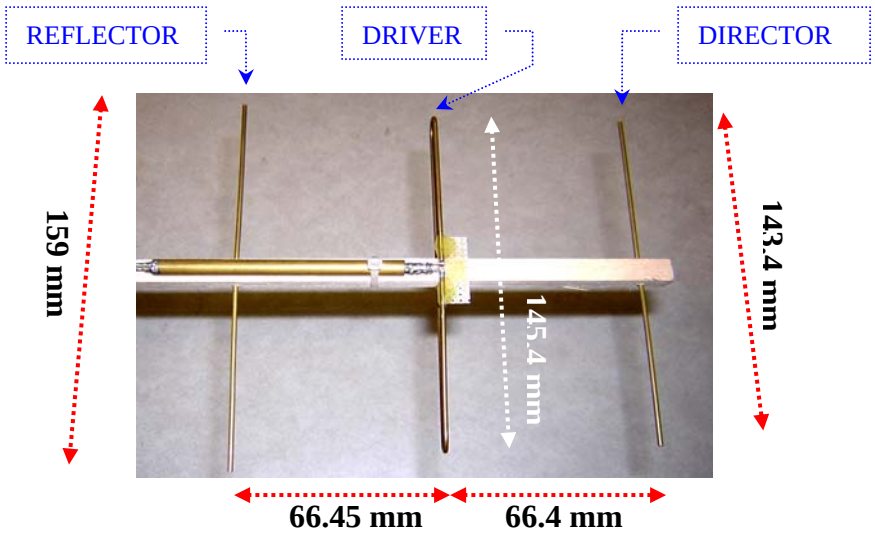

Figure 10. Tree element folded dipole yagi antenna .

a. Directivity and Gain

Directivity, gain, and radiation intensity are the main instruments denoting the capability of an antenna to focus power in a specific direction. Directivity is a function of the power radiated by an antenna, while gain relates to the power delivered to the antenna by the transmitter.[18] Though they are both angle dependent (i.e., function of θ and φ in polar coordinates), gain refers to the direction of maximum radiation. Similarly, the directivity of an antenna can be defined as the ratio of maximum power density ($P(\theta,\varphi)$) to isotropic power density ($P_{isotropic}$). This ratio is usually expressed in decibels [11]

$$D(\theta,\varphi) = 10 \ log[\frac{P(\theta,\varphi)}{P_{isotropic}}] \quad dB \tag{2.1}$$

The directivity is related to gain ($G(\theta,\varphi)$) as;

$$G(\theta,\varphi) = \gamma D(\theta,\varphi) \tag{2.2}$$

where γ refers to the radiation efficiency and is equal to the ratio of radiated power to the delivered power. [18] The power density is always dependent on the orientation of the receiver, which is measured in polar coordinates. The direction of maximum power

density is assigned to $\theta = 0$, $\varphi = 0$. This orientation is known as the foresight of the antenna. [11, 18]

b. The Effective Area of Folded Dipole Yagi Antenna

The effective area of the antenna measures how well the antenna captures power, and is simply the ratio of the power received by the antenna to the power density at the point where the antenna is located. The effective area of the antenna can be much larger than the antenna's geometric area. The effective area of an antenna (A_{eff}) is related to the antenna gain by the following formula [11]

$$A_{eff} = G(\theta,\varphi)\cdot\frac{\lambda^2}{4\pi} = \frac{P(\theta,\varphi)}{P_{isotropic}}\frac{\lambda^2}{4\pi} \qquad (2.3)$$

where $G(\theta,\varphi)$ is the antenna gain, $P(\theta,\varphi)$ is the maximum power density and $P_{isotropic}$ is the isotropic power density. [11] The effective area of the folded dipole antenna in our system is then calculated as $0.035m^2$ in the foresight where φ and θ are both zero.

2. Antenna Radiation Patterns

A radiation diagram describes the ratio of the antenna's power density at any orientation around the antenna to the isotropic power density: i.e., gain of the antenna in this direction. Even though the term radiation is used, radiation patterns are also applicable to an identical receiver antenna due to symmetry. [18] Two dimensional patterns that indicate the E-field and H-field planes are usually satisfactory for determining the directional characteristics of an antenna. [11] Radiation patterns are obtained for the folded dipole Yagi antenna by using a 915 MHz RF generator and LVDAM-ANT software as depicted in Figures 11 and 12 (also see Table 1 for numerical values).

Plane	Attenuation (dB)	Maximum Signal		Half Power Beam Width (^{o})
		Level (dB)	Position(^{o})	
E	10	-4.5	2	59
H	10	-2.2	0	85

Table 1. Folded dipole Yagi antenna radiation pattern properties.

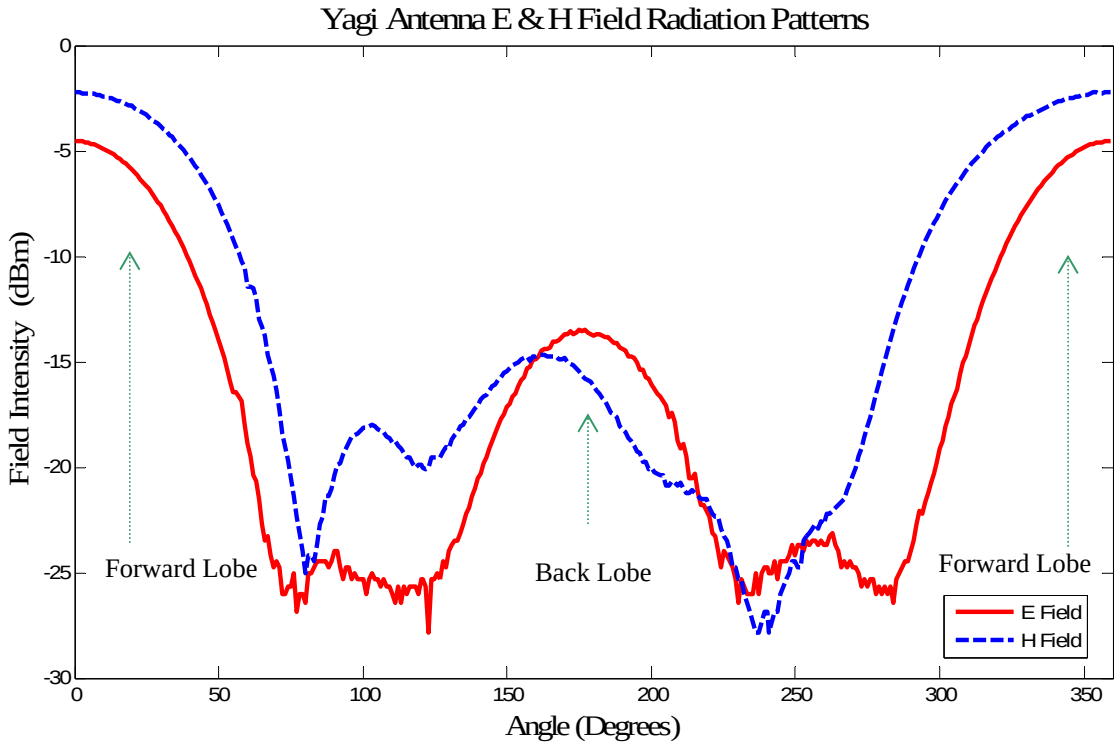

Figure 11. Yagi antenna radiation patterns for E and H-fields.

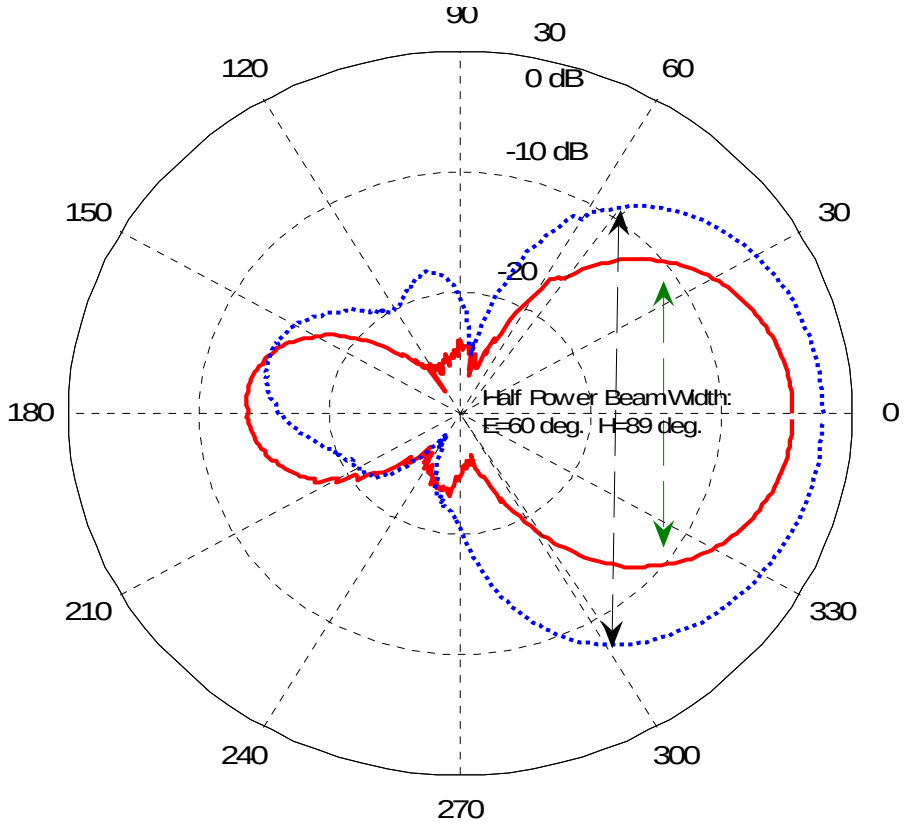

Figure 12. Radiation patterns in polar coordinates.

3. Antenna System SWR

Voltage standing wave ratio (VSWR), or simply SWR, which represents the ratio of maximum radio-frequency voltage to minimum radio-frequency voltage through a transmission line or an antenna, is a mathematical expression used to indicate the electromagnetic field variations on the transmission line. Similarly, a ratio of maximum and minimum RF currents on the antenna wiring yields the current standing wave ratio ISWR, which is basically the same as VSWR. It is a measure of reflection or impedance match.

For the ideal case, the RF voltage is required to be the same at all points on the signal transmission line. This results in an SWR of 1:1. Since the denominator is always unity, SWR is usually expressed in terms of the numerator (i.e., SWR=1 for the ideal case). This most favorable situation can be achieved only when the impedances of the load (antenna) and the transmission line match. More explicitly for an SWR of 1, antenna

resistance must be the same as the impedance of the transmission line, and the antenna must also be free of inductance or capacitance. All of the RF power that is sent by the transceiver is utilized by the antenna in the form of EM-field radiation when the SWR is equal to 1. In cases where SWR >1, a certain amount of transmitted RF power reflects back from the connection point to the antenna. The SWR is also connected to the ratio of these reflected and forward powers. Mathematically, SWR is given by [3, 11]

$$SWR = \frac{V_{max}}{V_{min}} = \frac{1+|\Lambda'|}{1-|\Lambda'|} \tag{2.4}$$

where Λ' is the voltage reflection coefficient which is equal to Λ' = (power with load/power without load) $^{1/2}$. In equation 2.5, (1-$|\Lambda'|^2$) represents the percent of radiated power delivered to the antenna. The mismatch loss is then equal to

$$\text{Mismatch Gain Reduction (dB)} = -10\log(1-|\Lambda'|^2) \tag{2.5}$$

The impedance match can be checked indirectly by measuring the SWR of the antenna system. The reflected power should be less than 10% of the forward power. [9] Thus, the following procedure is followed to measure the standing wave ratio of the folded dipole Yagi antenna between the frequencies 902-928 MHz:

- A directional wattmeter is placed between the antenna connector and the transceiver after the calibration process is completed.
- The access point is put into the radio test mode, which lasts ten minutes. (The radio test mode can also be terminated manually before ten minutes.)

  (***Main Menu>Maintenance Menu>Radio Test>Test Mode>Y>ON)***
- The transmitter power is set to 30 dBm with the following sequence of menus.

  (Main Menu>Maintenance Menu>Radio Test>Test Mode>Tx Power Output)
- TxKey function is turned on.

  (Main Menu>Maintenance Menu>Radio Test>Test Mode>TxKey> Enable)

- Forward and reflected power into the antenna system is measured; SWR and power output level is calculated by HP8510C. The output is recorded between the frequencies 902-928 MHz. Frequency range between 930-965 MHz is additionally evaluated by using HP8510C to test the performance of Yagi antenna at higher frequencies.

The recorded SWR data for the three-element folded dipole Yagi antenna is plotted using a computer program as depicted in Figure 13. According to SWR data, the ideal operational frequency for maximum performance is observed to be 910 MHz. The frequency range for the condition SWR<2 is determined to be 902 MHz<f <917MHz, as seen in Figure 13. SWR for 915 MHz is measured as 1.7, which causes a gain reduction of 0.3 dB (see Figure 14).

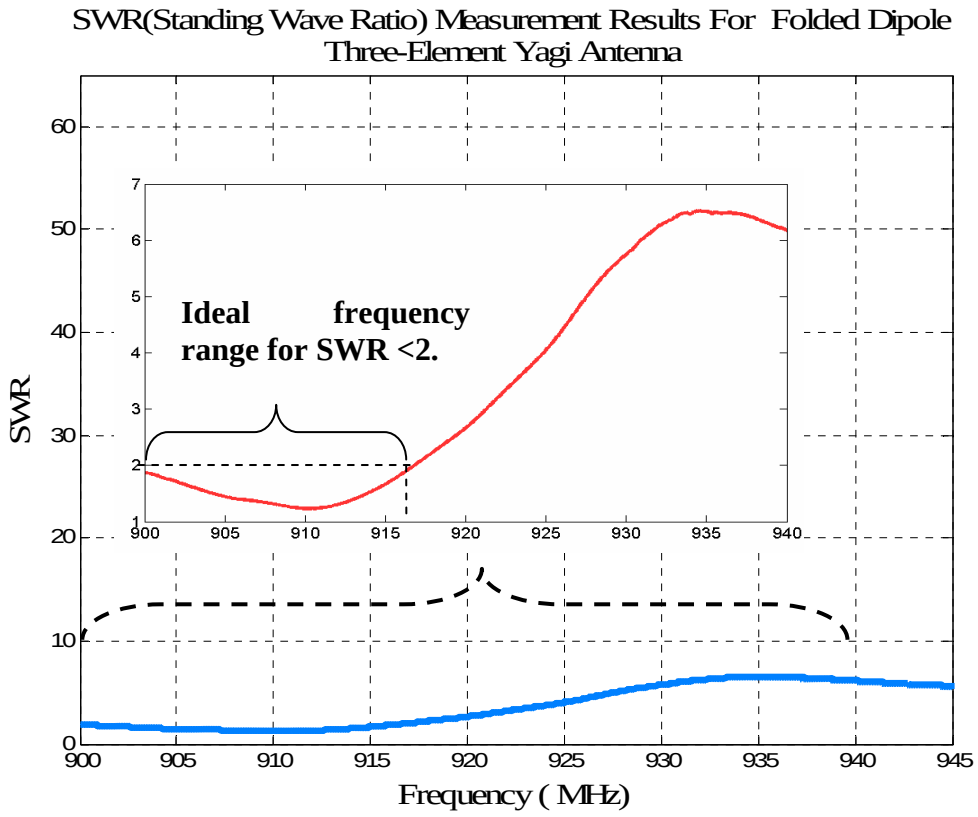

Figure 13. SWR plot for folded dipole Yagi antenna.

From equation 2.4 the following expression is obtained

$$|\Lambda'| = \frac{SWR-1}{SWR+1} \tag{2.6}$$

Then, the power reflection coefficient $|\Lambda'|^2$ (i.e., percentage of reflected power) is calculated from the measured SWR values and plotted as a function of SWR as shown in Figure 14 (dashed line). Mismatch gain reduction is calculated by using equation 2.5 and plotted in Figure 14 (dotted line).

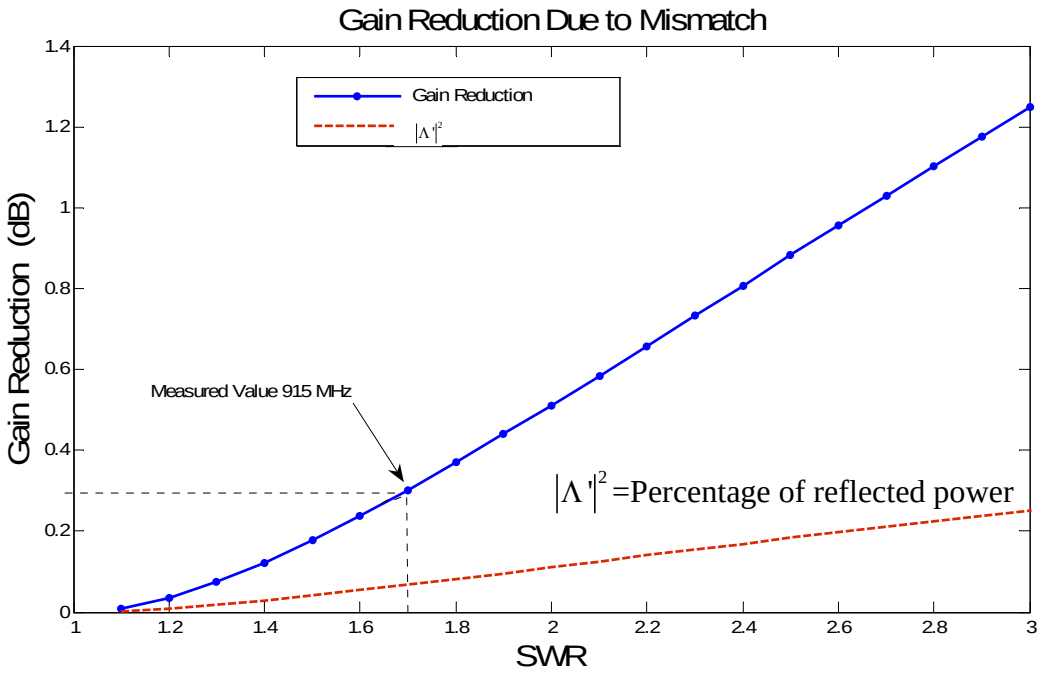

Figure 14. Gain reduction on Yagi antenna due to mismatch is marked with an arrow.

D. SYSTEM GAIN AND EFFECTIVE RADIATED POWER

Antenna system gain is a value which represents the power increase resulting from the use of a gain-type antenna. System losses from the feedline and coaxial connectors are subtracted from this figure to calculate the total antenna system gain as shown in equation 2.7. Then ERP (or EIRP) is related to system gain as defined in equations 2.7 and 2.8

$$G_{sys}(dB) = G(dBi) - L_{feedline}(dB) \quad (2.7)$$

$$ERP(dBm) = G_{sys}(dB) + Transceiver\ Output\ Power\ (dBm) \quad (2.8)$$

In the U.S., the maximum allowable EIRP level is 36 dBm (4 Watts). Thus, for our case, any antenna with a gain of 6 dBi or less allows us to utilize the maximum output power of the iNET 900 transceiver, which is 30 dBm (1 Watt). Regarding the five-foot long feedline cable, $L_{feedline}(dB)$ is found to be 0.195 dB and gain loss due to impedance mismatch is 0.3 dB (see Figure12). System gain (G_{sys}) is then calculated as 5.505 dB. When the maximum output of the transceiver is used, a maximum EIRP level of 35.5 dBm (3.55 Watts) can be obtained.

E. CONNECTIONS

1. IR-160 Camera Connection

The IR-160 camera provides a serial data output and can be reached through the RS-232 data link. Thus it is connected to the COM1 port (30010) of the modem. A serial connection to the camera from a computer is possible via any emulating terminal program such as Hyper Terminal in Windows. For Windows users, the following steps should be followed to configure the camera:

Start → All programs → Accessories → Communications → Hyper Terminal

A connection to the camera is established via Hyper Terminal with the settings as shown in Figure 15a. After a connection is established, the thermal imager can be controlled by typing the commands provided in Appendix-B into the Hyper Terminal window. To download a captured image to the host computer, the steps depicted in Figures 15b and 15c should be followed. [1]

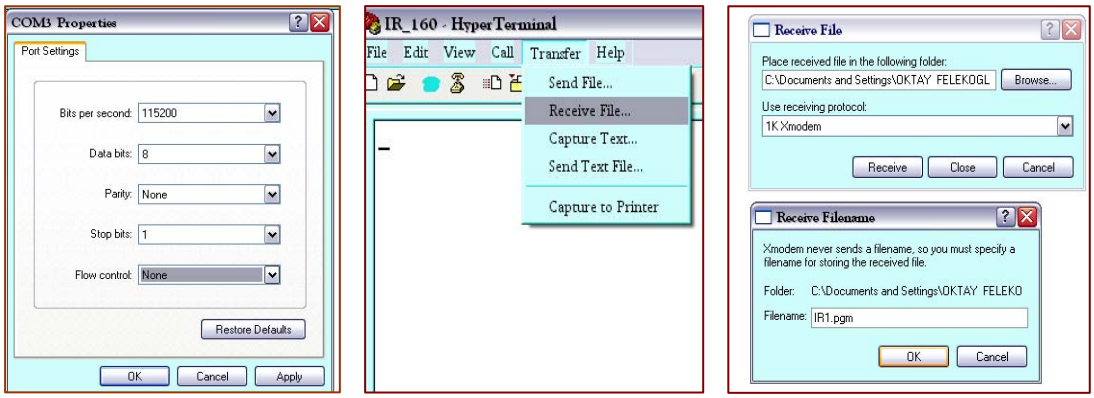

a) **b)** **c)**

Figure 15. a) IR-160 Thermal Imager Hyper Terminal connection settings for serial connection. b) Downloading captured IR image to host computer via Hyper Terminal. c) File settings for downloaded bitmap file.

2. Transceivers

The MDS transceivers can be accessed and configured through a menu-based management system which also provides basic diagnostic and maintenance tools. There are three methods to reach the embedded management system of the transceiver. [1, 9]

The first method requires connecting via a terminal emulator program such as Hyper Terminal. A serial data link is built between COM1 and the computer on which the emulator program works. Data baud rate should be set to 19200 bps in Hyper Terminal settings differing from the IR160 settings. The second method utilizes Telnet to access the management system through a network connection to the transceiver's LAN port. The third method uses a web browser, which requires a LAN connection with a crossover CAT-5 ethernet cable. Addresses for the access point and the remote are http://192.168.1.1 and http://192.168.1.3 respectively. Before connecting to the LAN port, transmission control protocol (TCP/IP) properties of the computer should be set according to the assigned IP addresses of the transceivers. In all three methods, a login page will appear in the first connection asking for a username and password. Default username and password are set as "iNET" and "admin" respectively. Main menu

components are depicted in Figure16a. Radio and serial port configuration parameters are set as shown in Figures 16b and Figure 16c.

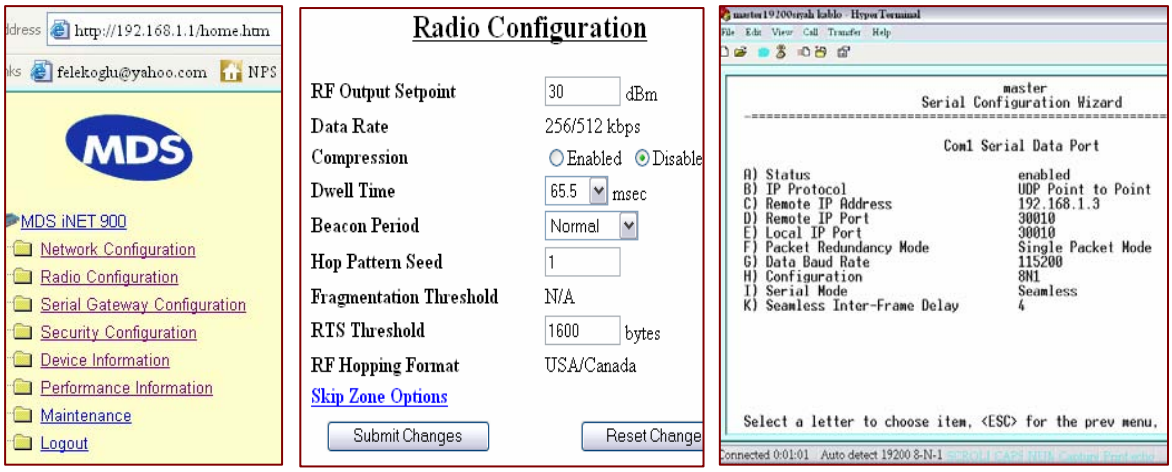

a) **b)** **c)**

Figure 16. a) Menu elements of the management system when connected via an HTTP browser. b) Radio configuration parameters as displayed on the HTTP browser c) COM1 Serial Data Port configurations as displayed on the Hyper Terminal.

THIS PAGE INTENTIONALLY LEFT BLANK

III. EXPERIMENTAL SET UP

The primary purpose of the experiment was to determine how well the IR image transfer system would perform under real combat conditions. Therefore, the effects of obstructive separating media, like foliage, buildings, natural terrain irregularities, etc., on image transfer were investigated. To get a good sense of the system performance, repeated measurements were taken through these separating media. The difference between transmitted and received power levels indicated the expected loss level in a similar combat zone. Path loss through the free space was measured as a reference for data comparison. The measurements included the image transfer through buildings and common building materials. The received signal strength level was read from the built-in performance indicator of the transceivers and compared to the transmitted power. Because determining the success level of the image transfer was more important than merely figuring out the path loss for different media, a probabilistic file transfer performance analysis was also conducted.

1. Equipment Setup

The experimental set up was comprised of:

- A transmit and receive unit,
- Two folded dipole Yagi antennas,
- A computer terminal for data recording and monitoring,
- An HP8510C network analyzer,
- HP8562 spectrum analyzer,
- A GPS unit
- Power supplies for the transceivers.

The IR160 camera was used during the indoor measurements. Outdoor measurements were completed with the help of text files with identical characteristics to the PGM files, due to the outdoor power limitations of the camera.

The transmitted and received power levels were first measured by the HP8562A spectrum analyzer in the lab environment to check the accuracy of the internal received signal indicator of the transceiver. After the accuracy of the built-in RSSI indicator was confirmed, transmission data through different media with different scenarios was collected using the set-up shown in Figure17. Data was recorded with the help of the Hyper Terminal Log.

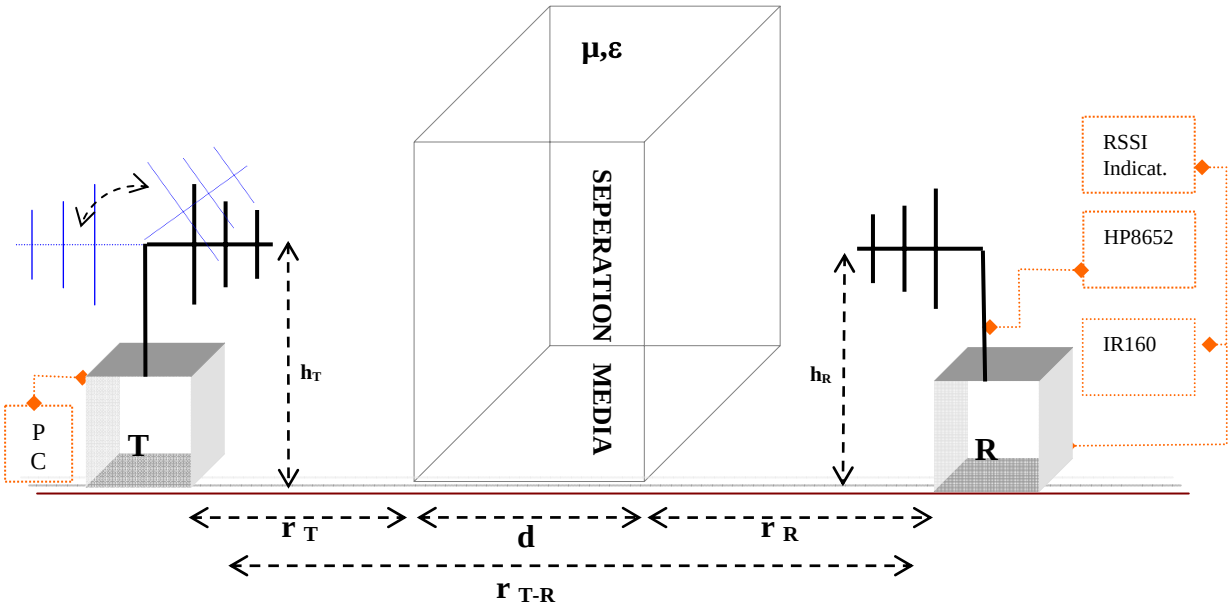

Figure 17. Experimental set-up geometry.

2. Description of the Measurement Environment

To increase the accuracy of the measurements, the file transfer performance data was taken in the NPS anechoic chamber. This decreased the error caused by reflected and multipath wave components to an acceptable level. Interference from adjacent units sharing the same ISM band was also reduced by the insulated walls of the anechoic chamber (Figure 18). Urban environment measurements were conducted at random locations in the cities Pacific Grove and Monterey Bay, which encompass an area of 45 km by 7 km. Open field measurement sites were chosen to satisfy different cases of data link obstruction. It is highly possible that data link obstruction would be encountered in a combat communication.

Figure 18. Sample images from anechoic chamber and foliage data collection processes.

Foliage and tree data were collected at the NPS campus. A 1000 m range of dense and semi-dense foliage was available. Additionally, various buildings at NPS, like the Dudley Knox Library, Ingersoll Hall and Watkins Hall, which have large strong reinforced cement volumes, were tested to determine the overall building penetration capability. Indoor measurements consisting of wall penetration and floor penetration were completed in Spanagel Hall.

3. Measurement Process

The transceiver has a built-in received signal strength indicator (RSSI) that is used to indicate when the antenna is in a position that provides the optimum received signal strength (Figure 19). RSSI measurements and wireless packet statistics are based on multiple samples over a period of several seconds. The average of these measurements is displayed by the management system. [9]

While collecting data using the built-in RSSI indicator, the following steps were taken:

- Remote transceiver association with the access point was verified by observing the status of link led.

  LINK LED = On or Blinking

  This indicated that we had an adequate signal level for the measurements and it was safe to proceed.

- Wireless Packets Dropped and Received Error rates were viewed and recorded via Hyper Terminal Log.

  (Main Menu>Performance Information>Packet Statistics>Wireless Packet Statistics)

- Wireless Packets Statistics history was cleared beforehand.

  (***Main Menu>Performance Information>Packet Statistics>Wireless Packet Statistics>Clear Wireless Stats)***\

- The RSSI level at the remote station was recorded.

  (Main Menu>Performance Information>RSSI by Zone)

- By slowly adjusting the direction of the antenna, the RSSI level (less negative was better) was optimized. RSSI indication level was watched for several seconds after making each adjustment so that the RSSI accurately reflected any change in the link signal strength.

- Wireless Packets Dropped and Received Error rates were viewed at the point of maximum RSSI level.

  (Main Menu>Performance Information>Packet Statistics>Wireless Packet Statistics)

An increase in the wireless packets dropped and received error at the RSSI peak indicated the possibility of the receiver antenna misalignment to an undesired signal source.

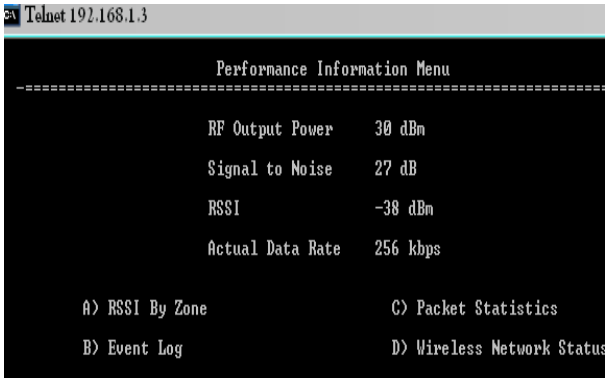

Figure 19. Performance information menu of the transceiver's management system.

4. Measurement Units

Received Signal Strength Indicator (RSSI), miliwatts (mW) and dBm are the most common measurement units utilized to indicate the strength of an RF signal. These measurement units are interrelated and each can be converted to one or both of the other measuring units with some alteration in precision.

a. dBm

The "dB" notation is generally used to represent gain or attenuation where logarithmic interdependence between input and output values is the most common case. In our system, the received power will always be related to transmitted power. The input signal is either augmented or diminished by a certain factor, which is represented in decibels. The +3 dB is twice the power, while -3 dB is one half the power. It takes 6 dB to double or halve the radiating distance, due to the inverse square law. The "dBm" notation represents a measured power level in decibels relative to 1mW. Since the EIRP of our system is 3.5 Watts, with antenna gain included, the dBm scale is preferred as the major measuring unit for our experiment.

b. Received Signal Strength Indicator (RSSI)

The RSSI indicates the received signal strength with regard to a reference output power. It is generally expressed in dBm units. RSSI is not a standardized unit; it

may change from application to application. Generally, commercial products have their own RSSI scales peculiar to the application. In our system, an RSSI level of 30 dBm indicates a transmitted power output of 1000 mWatts. Neglecting the feedline loss, the folded dipole Yagi antenna, with a 6 dB gain, quadruples the transmitted power. Due to the short distance loss, the RSSI level drops to -38 dBm at the beginning of the far field (Fraunhofer region).

IV. EXPERIMENTAL RESULTS

A. FILE TRANSFER MECHANISM PERFORMANCE ANALYSIS

1. The Effects of Transmitted File Size on System Capability

The IR-160 camera provides a portable bitmap image file with a changing size between 16 kb and 19 kb depending on the characteristics of the image. This image file is transferred to the computer's emulating terminal (i.e., Hyper Terminal) in the form of 20 data carrier packets which are recombined at the receiver to build an intact image file. For a successful image transfer, all 20 packets should be received at the receiver consecutively. An interruption in the transmittance process of data packets causes a corrupt file, which cannot be viewed by the browsing software. For our case, each data carrier packet is less than 1024 bytes (see Figure 20).

In our system, the carrier data packets which are the outputs of the IR-160 are sent to the transmitter unit as input data. Upon their arrival at the transceiver, the input data are transformed into UDP packets and are transmitted through the separating media and received at the access point. At this point, file size becomes a very important figure in determining system performance.

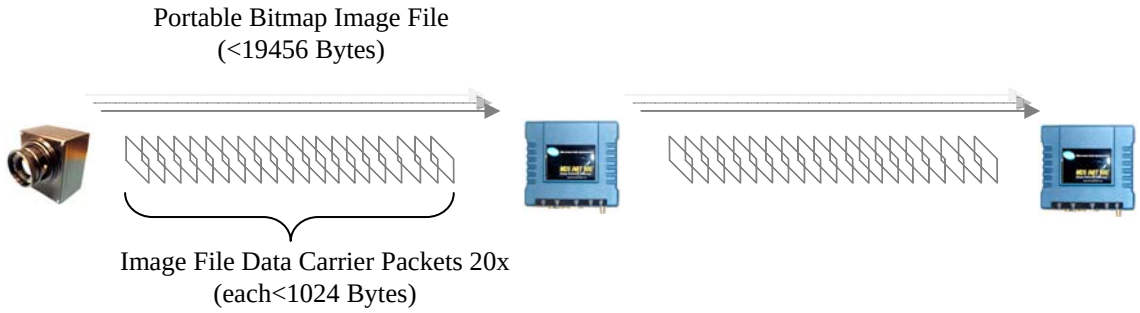

Figure 20. File transfer mechanisms for IR-160 and MDS iNET 900 transceivers.

In order to determine the effects of file size on transmittance capability in free space, different sized data packets ranging from 16 bytes to 22508 bytes were transmitted and received between the remote and access point units in the anechoic chamber. One hundred data packets were sent consecutively for each file size and an average

transmittance time was obtained for every file size. Each single dot in Figure 21 represents the average round trip time for the corresponding file size. Data transfer time seemed to be more stable for packet sizes less than 5 kb. Fluctuations in data transfer time were observed for bigger packets. This simply indicates that bigger data packets are more vulnerable to medium loss effects and attenuation. Changing medium conditions dramatically affects large file transfers.

Since each IR image file data packet is less than 1024 bytes in our system, we are in the safe region. During the anechoic room measurements (see Figure 16), no data packet loss occurred in our region of interest for IR image transfer. The approximate average time for a 1024 byte-data packet to be successfully transmitted between transmitter and receiver, in free space, is measured at 81.5 ms with a 2 meter T-R separation.

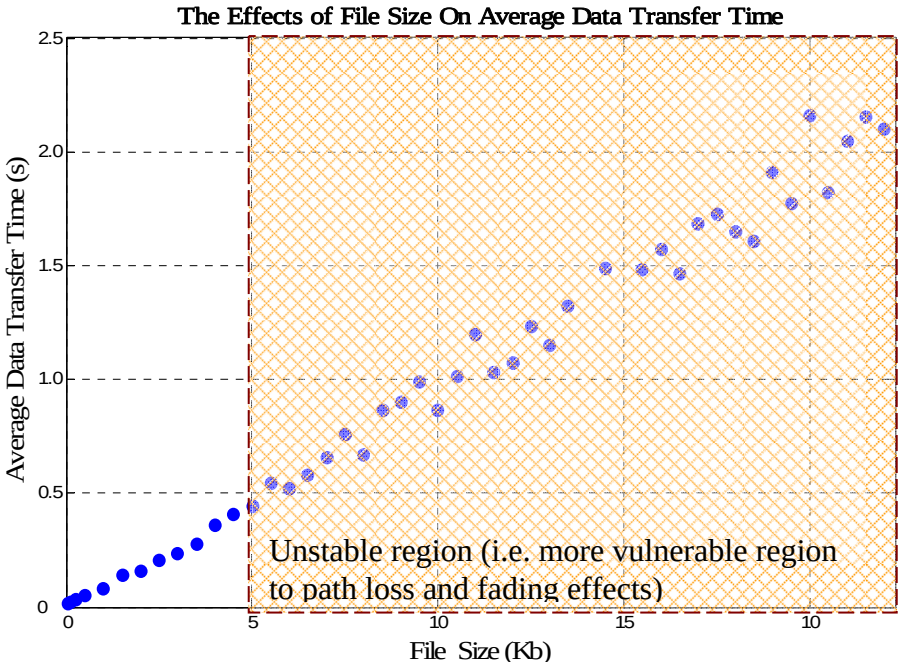

Figure 21. Data transfer time as a function of file size.

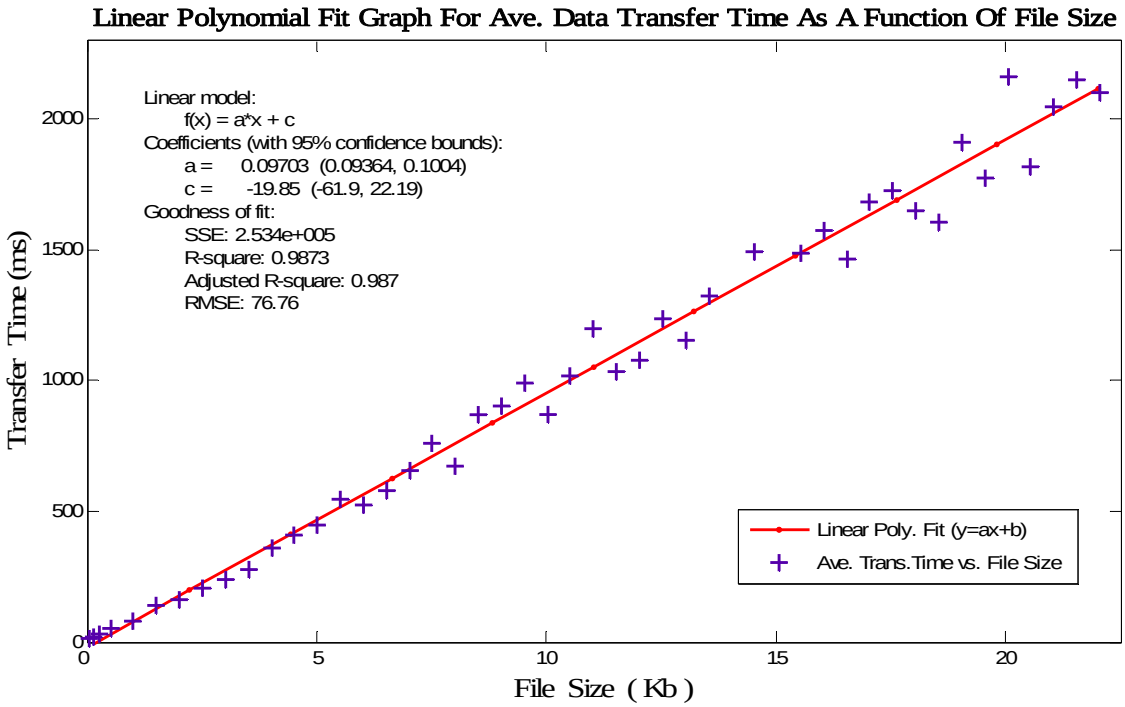

Figure 22. Linear polynomial fit graph for average data transfer time vs. file size (anechoic chamber).

The average data transfer time is found to increase linearly as the transferred file size increases, as seen in Figure 22. When a linear curve fit is applied to the experimental data the following expressions are obtained with an R-square value of 0.98

$$AFT\ (ms) = 0.10\ [FS\ (Bytes)] + 22 \qquad for\ FS < 512\ b \qquad (3.1)$$

$$AFT\ (ms) = 0.097\ [FS\ (Bytes)] - 19 \qquad for\ 512b < FS < 5000\ b \qquad (3.2)$$

$$AFT\ (ms) = 0.094\ [FS\ (Bytes)] - 62 \qquad for\ FS > 5008\ b \qquad (3.3)$$

where *AFT = Average file transfer time*

FS = File size.

Equations 3.1 and 3.2 are for the desired range for efficient file transfer. Using equation 3.2, the average transfer time for a 1024 byte file is calculated at 80 miliseconds, which correlates nicely with our measured data (see Figure 22). Therefore total transfer time for a standard IR image file of 19456 bytes is ≈ 4.5 seconds (20x 80 ms) after the three seconds of Hyper Terminal download time is included. However, it

should be understood that these measurements are conducted under the best communication conditions in an anechoic chamber at an RSSI level of -37 dB. Path loss and interference effects on file transfer time will be addressed in the following sections.

2. File Transfer Performance Measurements at Various RSSI Levels

In order to investigate the file transfer capability at different RSSI levels, standard 1024 byte-data packets were transferred, and average transfer times were recorded. Both outdoor and indoor measurement values were studied. The results are displayed in Figure 23.

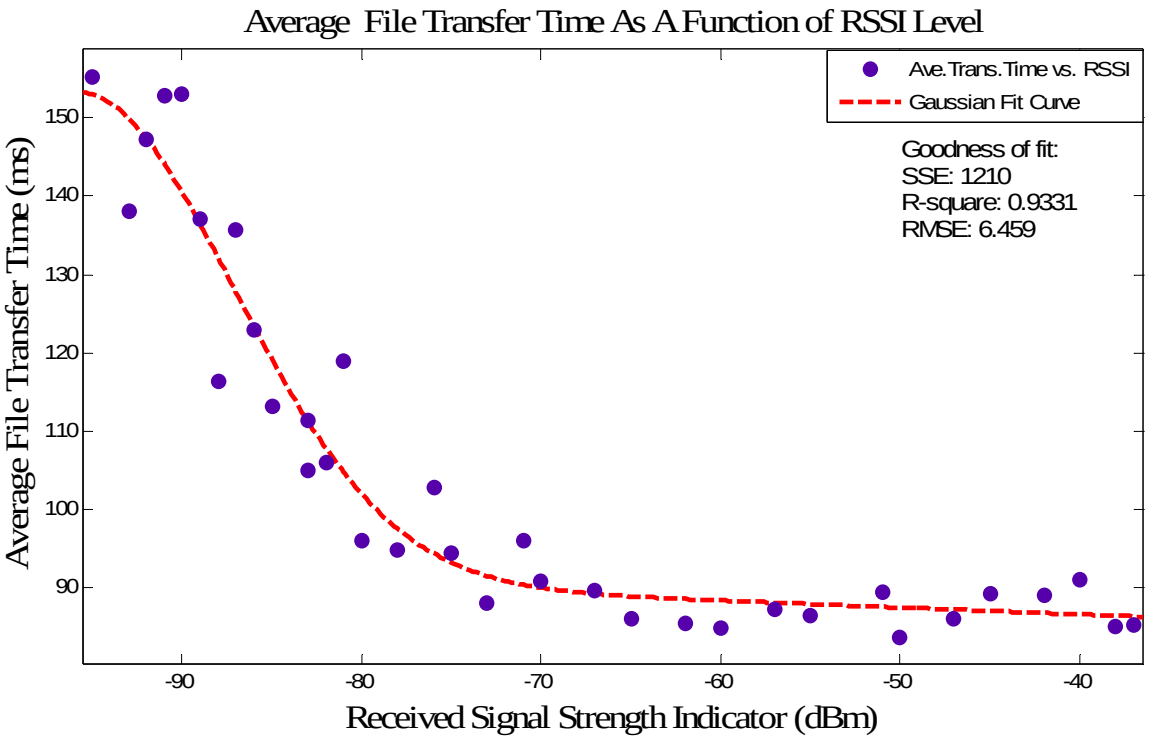

Figure 23. File (1024 bytes) transfer time as a function of received signal strength (open field data).

Measurements and curve fitting indicate that the average file transfer time, as a function of RSSI level, with 95 % confidence is given by

$$AFT(ms) = 62e^{-\left[\frac{(RSSI\,(dBm)+96)}{12}\right]^2} + 134e^{-\left[\frac{(RSSI\,(dBm)+907}{1311}\right]^2} \quad (3.4)$$

and further simplification results

$$AFT(ms) = 62e^{-\left[0.08\,RSSI\,(dBm)+8\right]^2} + 134e^{-\left[0.0008\,RSSI\,(dBm)+0.69\right]^2} \quad (3.5)$$

A sharp increase in file transfer time at RSSI levels lower than -75 dBm is observed in Figure 23. This indicates the susceptibility of file transfer at higher path loss levels.

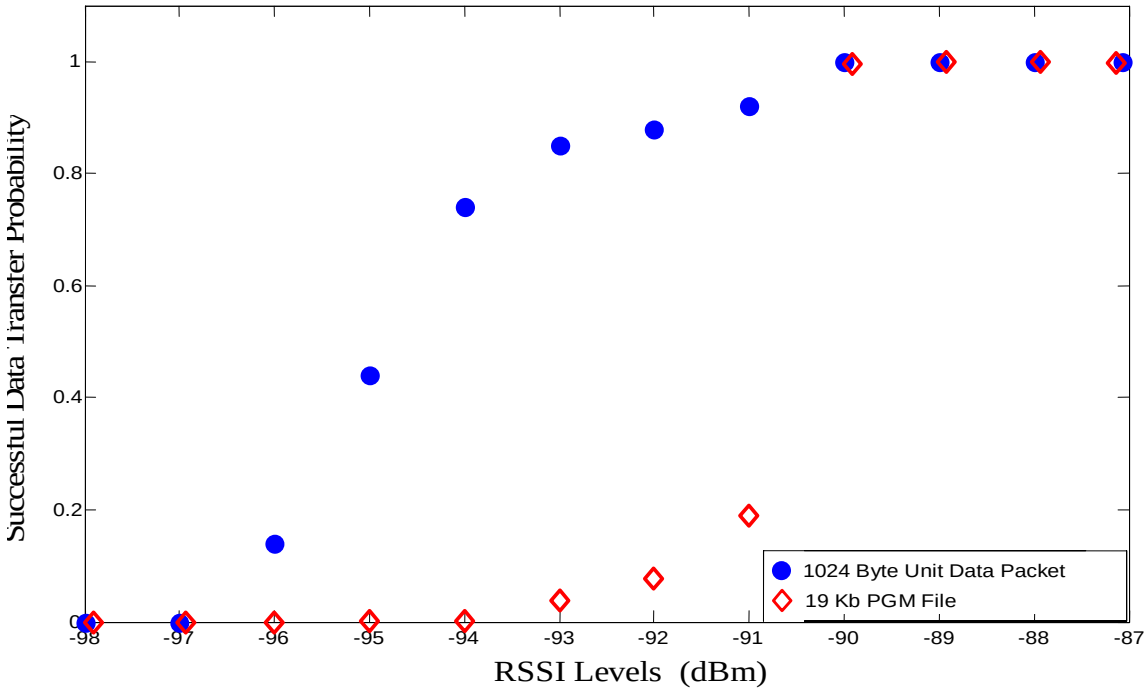

Figure 24. Successful data transfer probabilities at different RSSI levels.

Measurements revealed that data transfer has a probabilistic nature at lower RSSI levels (<-90 dBm). The probability plot in Figure 24 is obtained from the lost-delivered packet statistics of the transferred files and depicts the successful data transfer probabilities for the 1 kb data packets and 19 kb image file. Though the threshold RSSI value for a unit data packet to be successfully transferred (1 kb) can be approximated at

-94 dBm, it does not reflect the real image transfer performance. If the successful transfer probability of one unit data packet is $\hat{p}$, then 19 kb file transfer probability is $\hat{p}^{20}$, which will give considerably small values for $\hat{p}<1$ (see Figure 24).

At -94 dBm, which can be accepted as the minimum RSSI level for successful transfer (with a $\hat{p}$ value of ≈ 0.8) for a 1024 byte file, the average transfer time increases to 150 ms (Figure 23). An IR image file can be successfully transferred at -90 dBm. Even though the transfer might be possible at lower RSSI levels with low probabilities, -90 dBm can be considered as the limiting boundary for our system. Then, the worst case (-90 dBm) transfer of a 19 kb IR image file will take approximately 5.85 seconds. The difference in transfer times between the best and worst cases is accounted for by the path loss caused by the separating media plus interference and fading effects (Figure 25).

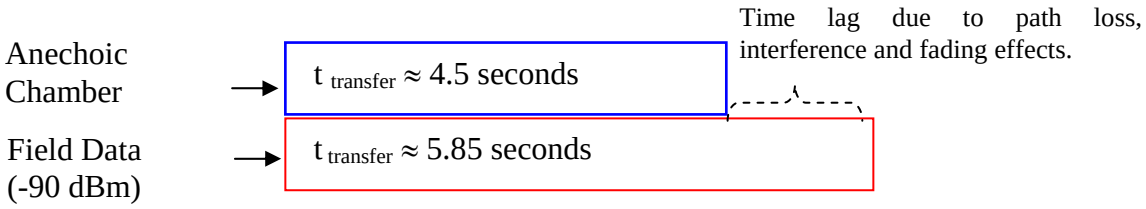

Figure 25. Time lagging in 19 kb PGM image file transfer due to path loss.

These file transfer times are important because they mark the limitation boundaries for “in-motion enemy detection capability” in active reconnaissance. Let us assume a simple scenario such that a reconnaissance team infiltrated into the enemy zone for surveillance and deployed an autonomous ground vehicle carrying an IR camera and a transceiver in order to observe enemy activities on critical routes. When the received signal strength level is -90 dBm, 10 images can be sent in one minute neglecting the operator’s speed while performing image transfer. When the first image (which scopes Frame 2 as shown in Figure 26) is taken at t = 0 s, the enemy tanks are still in Frame 1.By the time the system is ready to send the second shot , the target will have moved out of the imaging range.

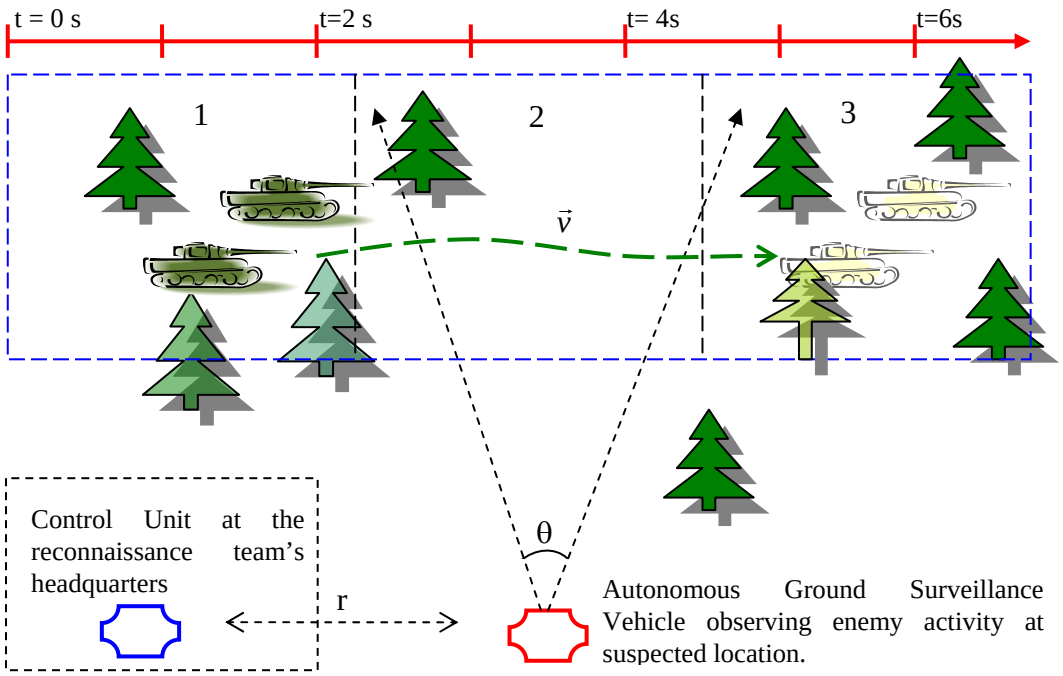

Figure 26. A simple combat scenario portraying the possible effects of file transfer system limitations on a surveillance mission.

3. Wireless Link Power Budget Analysis

Our wireless IR image transfer system operating at 256 kbps has a maximum transmission power of 30 dBm. The minimum received power value for successful operation was experimentally determined to be -94 dBm. The communication power budget is equal the maximum difference between transmitted and received powers

$$\textit{Power Budget (dB)} = P_{tmax}\,(dBm) - P_{rmin}\,(dBm) = 30\ dBm - (-94\ dBm) = 124\ dB$$

The maximum loss value that can be tolerated for successful image transfer is 124 dB. Notice that antenna gains G_T and G_R are absorbed in the value of -94 dBm. If antennas with unity gain were used, a minimum operation threshold would be -82 dBm.

4. Interference

Since the transceiver shares the radio-frequency spectrum with other 900 MHz services, near 100% error-free communications may not be achieved in a given site. Some level of interference should be expected. The best level of performance can be obtained on condition that care is taken in selecting unit locations with proper radio and network parameters. [9] Interference control techniques should be used in order to increase the system performance when setting up the data link between sensing and control units.

a. Interference Control Techniques

In rural areas systems are least likely to be affected by interference. In suburban and urban environments systems are more probable to encounter interference from adjacent devices operating in the license-free frequency band. [9]

Directional antennas confine the transmission and reception pattern to a narrow lobe, minimizing interference from the stations located outside the antennas' radiation pattern. For this reason, using directional antennas will help reduce the interference effects. If interference is expected from an adjacent system, it will be more convenient to use horizontal polarization of all antennas in the system. Since most other services use vertical polarization in this band, an additional 20 dB of reduction of interference can be obtained by using horizontal polarization. [9] A band pass filter can also be utilized to eliminate the unwanted interference signals. Reducing the length of data streams may also help decrease the interference effects. In the presence of interference, groups of short data streams have a better chance of getting through than do long streams. [9] Our image transfer system works in this manner, using 1 kb unit data packets instead of 19 kb files.

b. Interference Measurements

Interference was measured with the help of a built-in "received and dropped data packet statistics" menu on the transceiver (Figure 27). Using the ping utility certain numbers of data packages with fixed file sizes were sent continuously from the access point to the remote and vice versa for one-minute periods. Then the difference between the sent and received files was calculated from the records of Hyper Terminal Log. At some points the number and size of received files exceeded those of the sent files. This difference was assumed to be caused by the interference of the adjacent systems (Figures 28 and 29). Interference had adverse effects such as filling the buffer of the receiver and thus causing the data transfer fail. Data revealed that adverse effects of interference increased directly proportional to the increasing transferred file size (Figure 21).

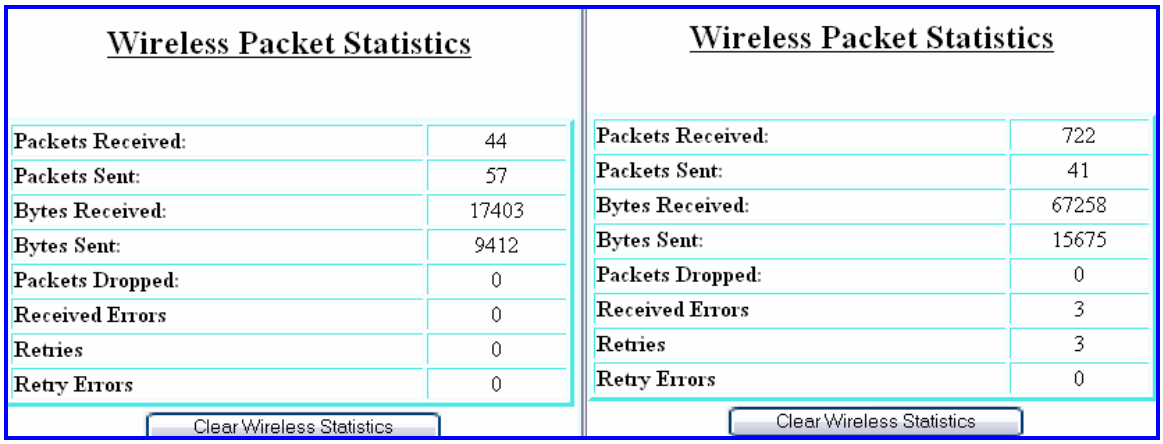

Wireless Packet Statistics

Packets Received:	44
Packets Sent:	57
Bytes Received:	17403
Bytes Sent:	9412
Packets Dropped:	0
Received Errors	0
Retries	0
Retry Errors	0

Clear Wireless Statistics

Wireless Packet Statistics

Packets Received:	722
Packets Sent:	41
Bytes Received:	67258
Bytes Sent:	15675
Packets Dropped:	0
Received Errors	3
Retries	3
Retry Errors	0

Clear Wireless Statistics

Figure 27. Wireless packet statistics menu of the transceivers as viewed from an HTTP browser, to the left is access point (master), to the right is the remote. Notice the difference between received and sent packets.

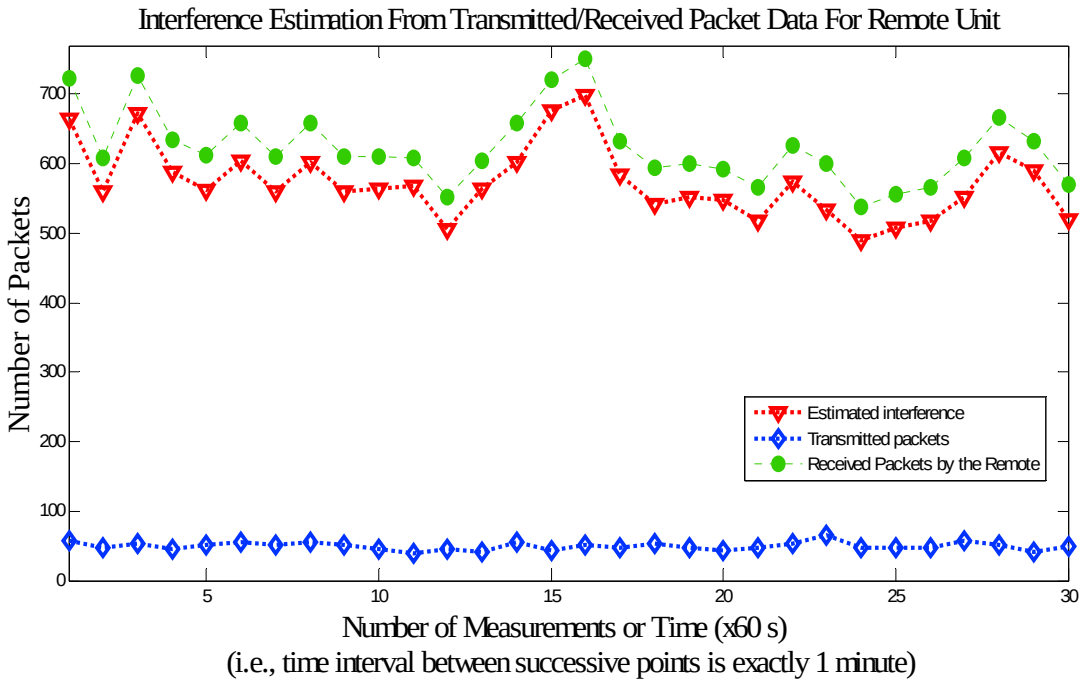

Figure 28. Interference data for the remote unit at -38 dBm.

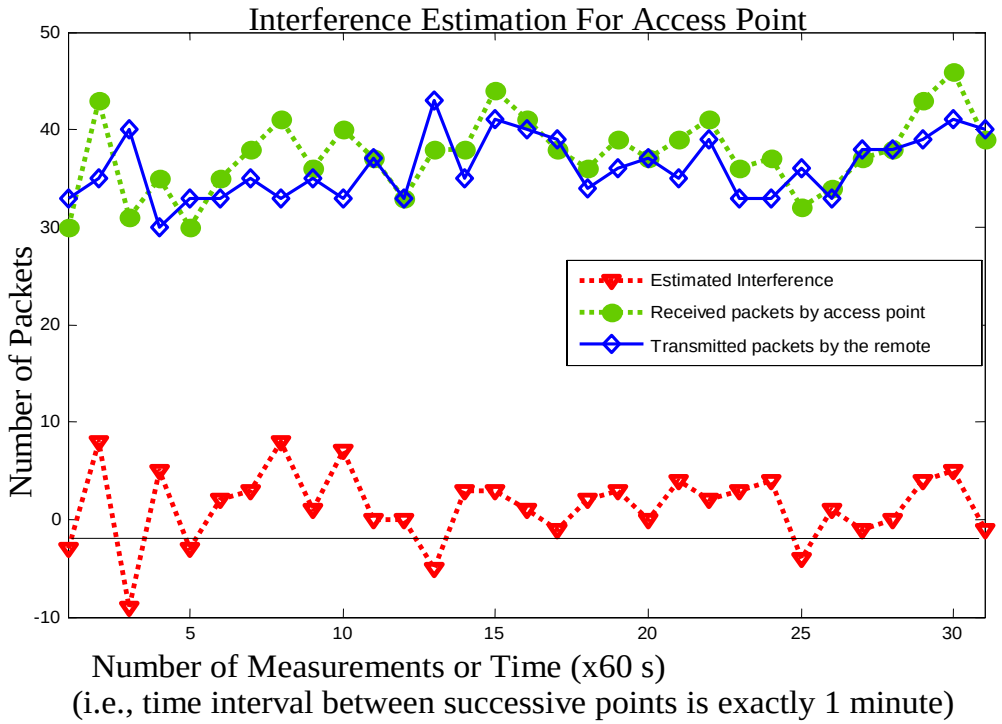

Figure 29. Interference data for the access point at -38 dBm.

A significant difference between remote and access point was observed in terms of the vulnerability to interference. The level of estimated interference for the remote unit was found to be 60-70 times higher than that of the master unit. Since the RSSI level at the time of the measurements was remarkably high (-38 dBm), minimal packet loss was suffered due to interference. But at lower RSSI levels, interference had a more deteriorating effect on packet loss. Various measurements were taken at different RSSI levels by shielding the transmitter antenna at the same location. However, the estimated interference level remained approximately the same for changing RSSI levels. When the measurement locations were changed, totally different interference levels were observed. The random nature of interference renders it highly unpredictable but for site specific interference measurements. In Figure 30 below, interference measurements for a remote unit at different sites are presented in order to characterize the location dependence of the interference. Data is again based on mutual sent received packet statistics between transmitter and receiver.

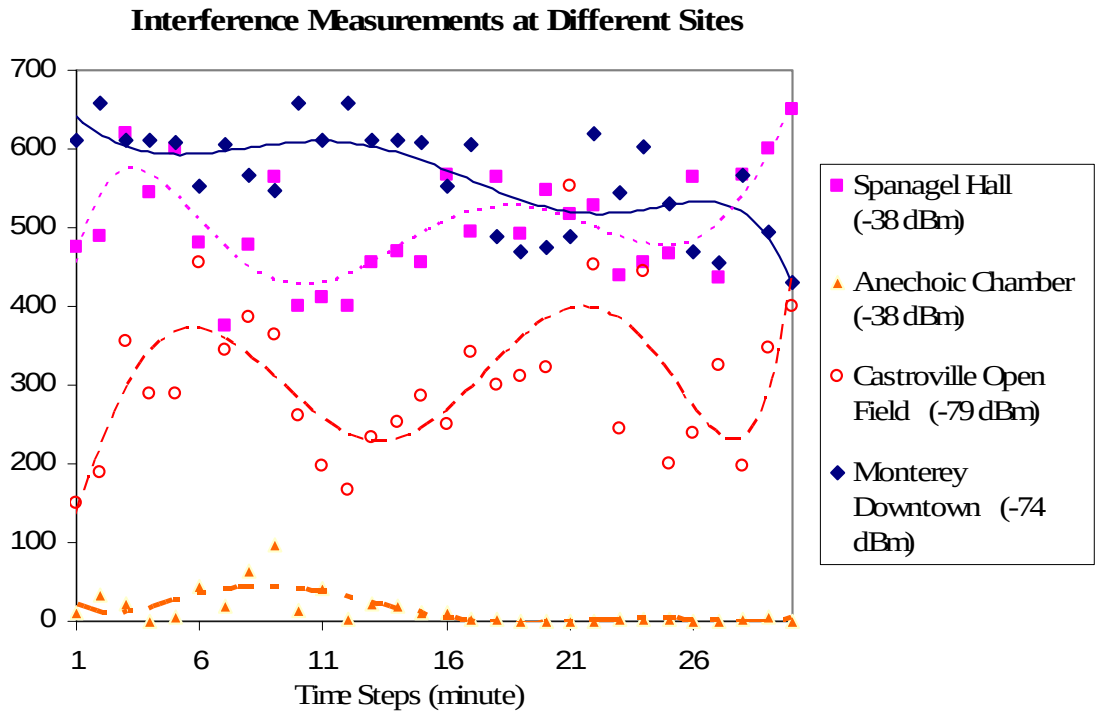

Figure 30. Sample interference estimates for different locations for remote unit.

B. OUTDOOR MEASUREMENTS

Outdoor measurements were conducted at random locations in the Monterey Bay and Pacific Grove areas in order to determine the line of sight (LOS) free space, urban and rural area communication capabilities of the IR image transfer system.

1. LOS/Partial LOS Free Space Measurements

If the shortest path connecting transmitter and receiver is not blocked by an obstruction, the communication between the end units is regarded as line of sight communication. However, as mentioned before in the introductory Chapter, the first Fresnel zone should also avoid the obstacles by 0.6 r_{F1} for the communication to be considered LOS in free space. Otherwise, diffraction caused by the edges of obstacles will also have effects on the communication characteristics. The maximum radius of the Fresnel zones occurs at the exact mid-point between the transceiver and the receiver. In order to check the path clarity for the LOS measurements, first Fresnel zone radii are calculated for the T-R separation values between 2 m and 50 km using equation 1.13 maximum (Figure 31).

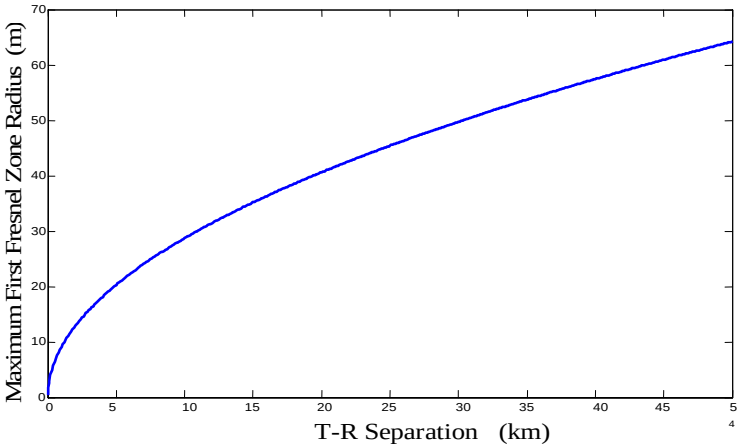

Figure 31. Maximum first Fresnel zone radii for T-R separations in interest.

The free space LOS measurements were carried out over the Monterey Bay which provided a very satisfactory range for healthy measurements with the convenient

geometry as described in Figure 32. The transmitter antenna was located on top of a building in Pacific Grove with an elevation of 53 meters from sea level.

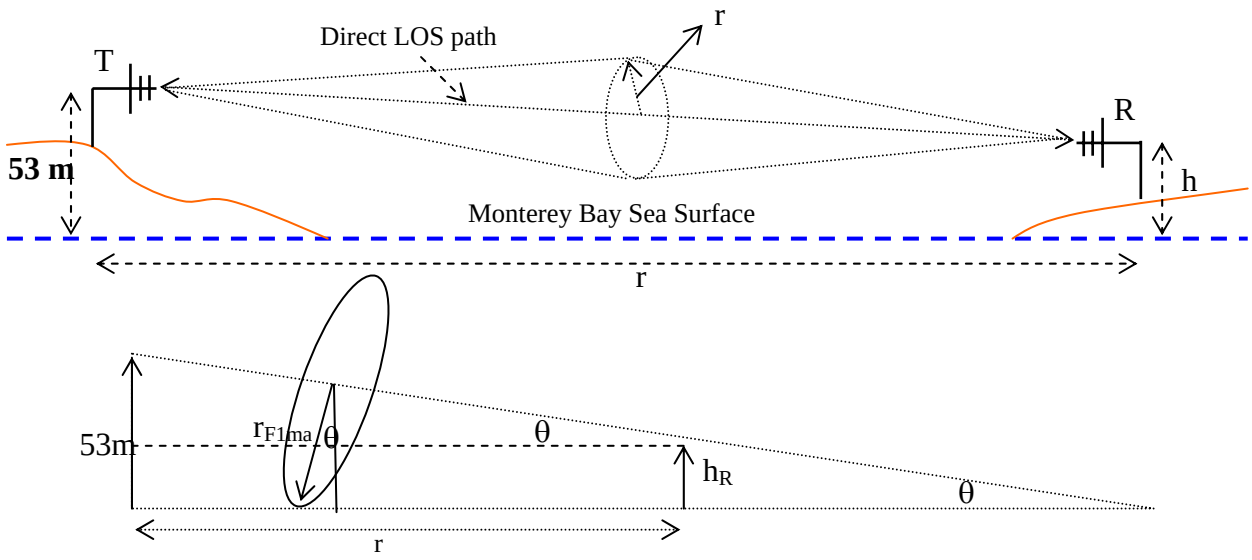

Figure 32. Free space LOS measurement geometry over Monterey Bay.

From the measurement geometry of our experiments, the following expression is derived in order to determine the path clarity for first Fresnel zone's over the Bay

$$\frac{r_{F1\max}}{h_T} = \frac{\frac{r}{2} + h_R \tan\theta}{h_R \tan\theta + \frac{3}{2} r} \tag{3.6}$$

where $\tan\theta = \frac{h_T - hR}{r} = \frac{2[h_T - r_{F1\max}\cos\theta]}{r} \approx \frac{2h_T - 2r_{F1\max}}{r}$

and further simplification will give

$$h_R + h_T = 2r_{F1\max} \tag{3.7}$$

This equation satisfies the condition in which the first Fresnel zone is barely touching the surface of the water. Since 0.6 r_{F1max} obstacle clearance is considered enough for free space communication and h_T is fixed all through the measurements then h_R should satisfy

$$h_R \geq 1.2(r_{F1\max}) - 53 \qquad (3.8)$$

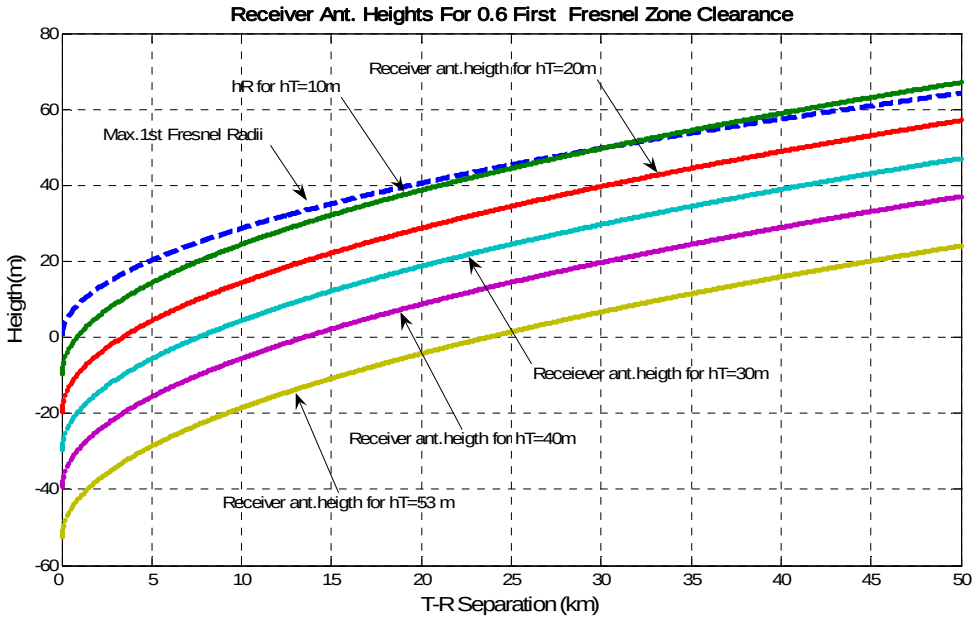

Figure 33. Minimum receiver antenna heights for 1st Fresnel zone path clearance.

Data collection sites were then chosen such that they would satisfy the minimum receiver antenna height requirements that were plotted for different communication ranges in Figure 33. Some sample measurement points for the LOS case were marked in Figure 34 located on the Monterey Bay beach line. For a few points (43, 31, and 37 in Figure 32) direct LOS path was satisfied, but first Fresnel path zone clearance criteria could not be fulfilled. These points were not excluded from main data, but are considered as partial LOS data.

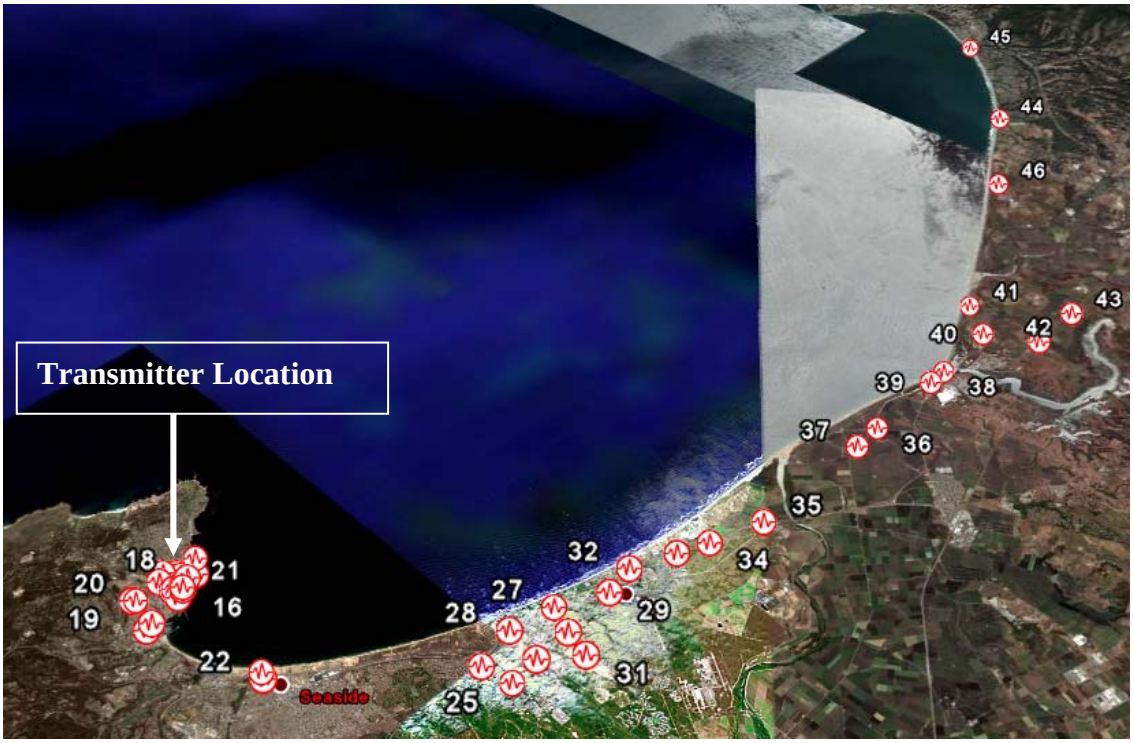

Figure 34. Monterey Bay outdoor measurement locations (image is obtained by Keyhole2LT software, Earthsat 2005, DigitalGlobe 2005).

a. T/R Separation

Results for the measured received signal strength levels are plotted as a function of transmitter – receiver separation (Figure 35). Various curve fit options were applied to the data in order to have a sense about the LOS free space characteristics of the system.

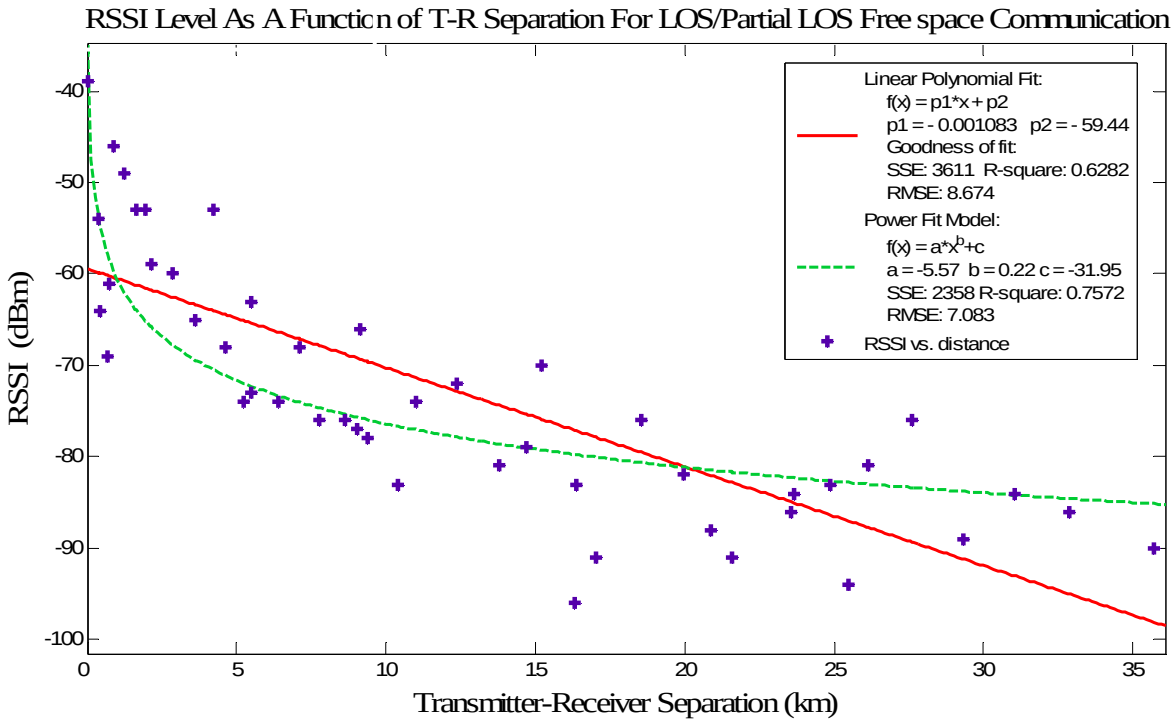

Figure 35. RSSI measurements at various T-R separation distances for LOS/partial line of sight free space communications.

A simple linear fit (R^2=0.62, i.e., fitted curve, explains 62 percent the objective data) applied to the data has the below indicated values

$$RSSI_{linear}\ (dBm) = -0.0019r\ (m) - 59 \tag{3.9}$$

Root mean square error for the data was calculated by

$$RMSE = \sqrt{\sum_{i}^{n} (P_{Ri} - \tilde{P}_{Ri})^2} \tag{3.10}$$

where P_{Ri} indicates the actual measured value for the received power, $\tilde{P}_{Ri}$ is the estimated value of the received power at distance r (m), and n is the number of measurements.

Root mean square error was then obtained for the linear fit as RMSE = 8.67 dBm. A power curve fit model yielded a better R-squared value of 0.75 and an RMSE value of 7.08 dBm

$$RSSI_{power} = -5.57r^{0.22}\ (m) - 31.95 \tag{3.11}$$

A normal distribution fit is also applied (Figure 36). The normal distribution has the form

$$\rho(RSSI) = \frac{1}{\sigma\sqrt{2\pi}} e \frac{-(RSSI - \tilde{\mu})^2}{2\sigma^2} \tag{3.12}$$

where $\tilde{\mu}$ is the mean value and is equal to

$$\tilde{\mu} = \frac{\sum_{i}^{n} RSSI_i}{n} \tag{3.13}$$

In equation 3.12, σ and σ^2 denote standard deviation and variance respectively, and σ is equal to

$$\sigma = \sqrt{\frac{\sum_{i}^{n} (RSSI_i - \tilde{\mu})^2}{n-1}} \tag{3.14}$$

The mean value of the measurements was then found to be -72 dBm with a standard error of 2 dBm (see Figure 36).

Standard deviation for the distribution was calculated as 14 dBm (standard error =1 dBm) and variance was then 198 dBm. Successful image transfer was conducted as low as -92 dBm occasionally; however an RSSI level of -90 dBm was proved to be a sturdier threshold for LOS free space communication. The area under the curve sums up to one, then the area to the right of -90 dBm lines gives us the successful image transfer probability for the given data.

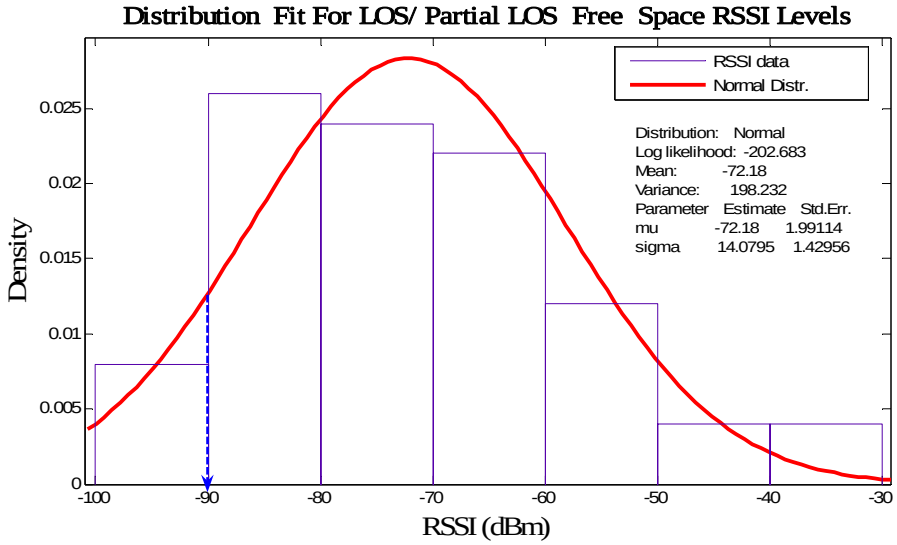

Figure 36. Normal distribution fit for line of sight/partial line of sight measured free space RSSI levels. The area under the curve to the right of the arrow (-90 dBm level) indicates the successful image transfer probability within a radius of 36 km.

b. Antenna Orientation Effects on RSSI Level

As the distance between the Access Point and remote unit increases, the influence of terrain, foliage and man-made obstructions becomes more influential and the use of directional antennas at remote locations becomes necessary. Directional antennas usually require some fine-tuning of their orientation to optimize the received signal strength.

Measurements showed that antenna disorientation may affect RSSI levels up to 15 dBm in an open field. Measurements were taken in free space LOS with a T-R separation of r = 200 m. Measurement results are represented on the next page (see Figure 37). For larger distances antenna orientation was observed to cause more severe effects on RSSI.

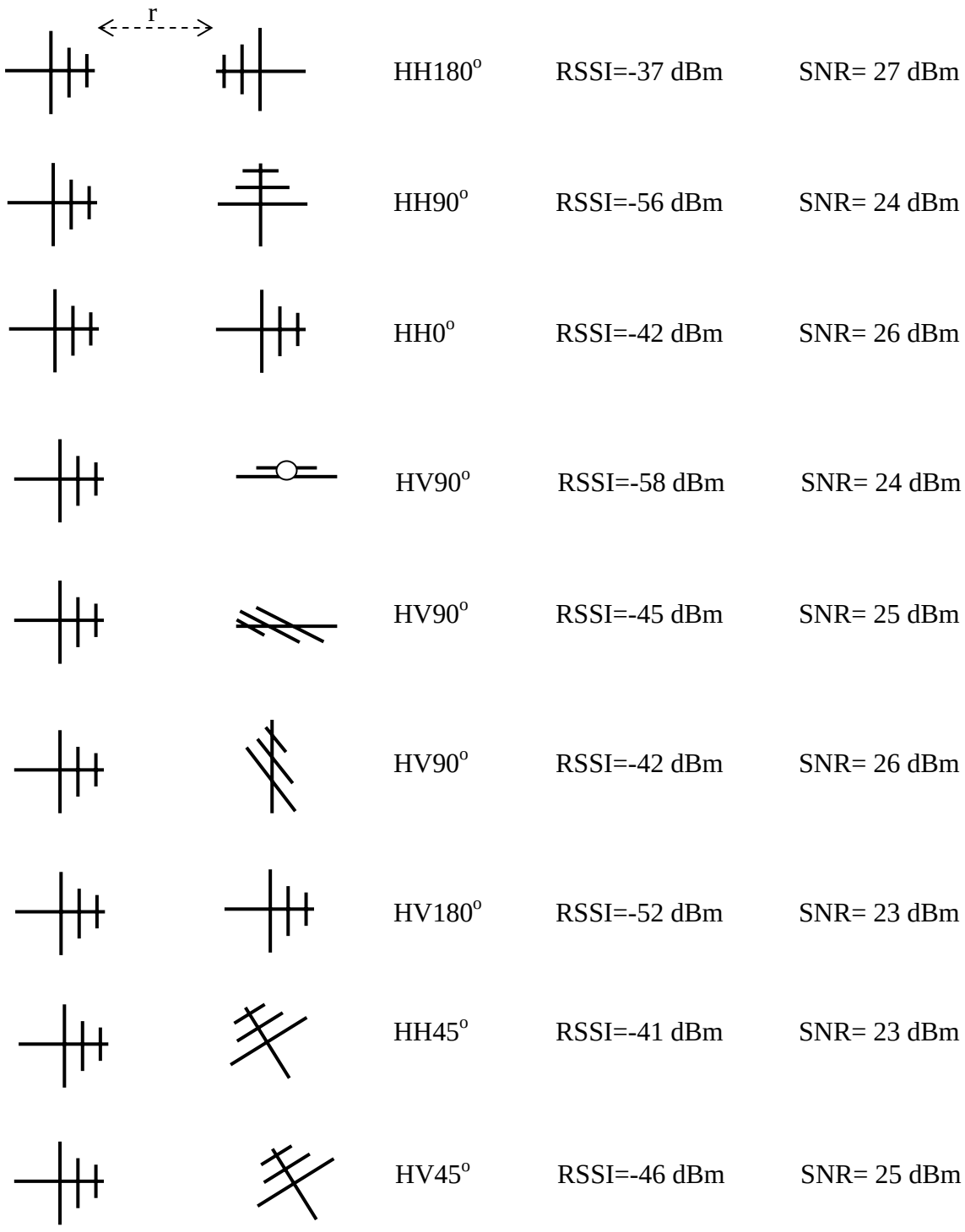

Figure 37. RSSI levels observed at different antenna orientations (horizontal-horizontal polarization (HH), horizontal –vertical polarization (HV)).

c. Maximum Free Space Communication Distance

The maximum free space communication range for a 915 MHz wireless link can be theoretically calculated by equating the power budget value (124 dB) to the loss value in equation 1.12

$$124dB = 32.45 + 20\ \log f(915MHz)\ +\ \ 20\ \log\ r_{max}\ (km)$$

From this calculation maximum free space range is theoretically obtained as $r_{max} = 41.3$ km.

Maximum range for our system was tested experimentally between Capitola (Santa Cruz) and Pacific Grove in dry weather (Figure38). Transceiver and receiver remained connected as far as 40.8 km where RSSI level dropped to -96 dBm. Data files were successfully transferred with acceptable packet loss at a maximum range of 35.5 km at -92 dBm. The difference between theoretical and experimental value was due to multipath effects and destructive interference caused by reflections from even numbered Fresnel zones.

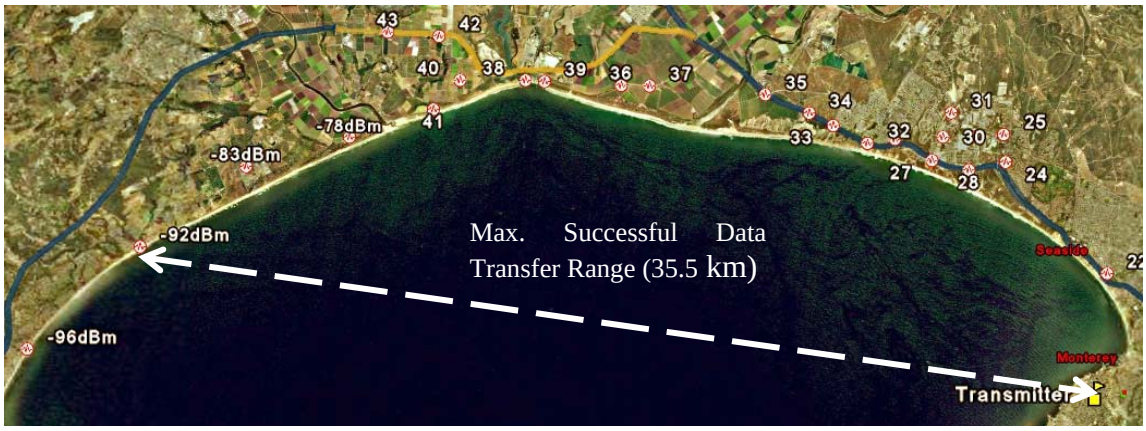

Figure 38. Maximum free space communication range.

2. Urban Area NLOS Measurements

In an urban or suburban environment, a direct LOS path between the transmitting and receiving antennas is not very common. Generally, multiple reflection and diffraction paths contribute the communication between a transmitter and receiver. Reflections from objects around the mobile antenna will originate multiple signals to add and cancel depending on the motion of the mobile unit. Nearly complete cancellation of the signal can take place, causing deep fades. These variations in the signal, which are on the order of tens of wavelengths, are named as small scale fading and predicted by Rayleigh statistics. [13, 14]

On a scale of hundreds to thousands of wavelengths the signal strength, when measured in dB, is found to be normally distributed; and is therefore referred to as a lognormal distribution. [13] The Hata model is used most often for predicting path loss in various types of urban conditions. Including correction factors for antenna heights and terrain, the Hata model is a set of empirically derived formulas. [12]

Figure 39. Sample urban area measurement points, Pacific Grove (image is obtained by Keyhole2LT software, Earthsat 2005, DigitalGlobe 2005).

The Hata model parameters [2, 11, and 12] are defined below

$$L_{median} = 69.55 + 26.16\log(f) - 13.82(h_T) + [44.9 - 6.55\log(h_T)]\log(r) + \xi(h_T) \quad (3.15)$$

where L_{median} is the median urban propagation loss, f is the frequency, h_T is the transmitter antenna's height and r is the distance between transmitter and receiver. In equation 3.15, $\xi(h_T)$ is the city correction factor and is equal to

$$\begin{aligned} &Medium\ \ city: \ \xi(\mathrm{h_T}) = [0.7 - 1.1\log(f)h_R + 1.56\log(f) - 0.8 \\ &L\arg e\ \ \text{city:}\ \ \xi(\mathrm{h_T}) = 4.97 - 3.2\log^2(11.75h_T) \quad \text{for}\ \ f \geq 400MHz \end{aligned} \quad (3.16)$$

Correction factors for suburban and open areas are defined as

$$\begin{aligned} L_{corr.sub.} &= -4\log(\frac{f}{28}) - 5.4 \\ L_{corr.open} &= -9.56(f) + 18.33\log(f) - 40.94 \end{aligned} \quad (3.17)$$

Total path loss is then given by

$$L_s = L_{median} - L_{cor}$$

Urban measurements were conducted in Pacific Grove, which was classified as a medium city. Sample measurement locations are marked in Figure 39. Transmitter antenna height h_T was 53 meters and fixed during the measurements. Measured path loss values are compared with the Hata urban propagation model in Figure 40. Experimental values complied with the Hata model for a medium city.

Root mean square error was calculated as 41.7 dBm, based on the estimated values from the Hata model.

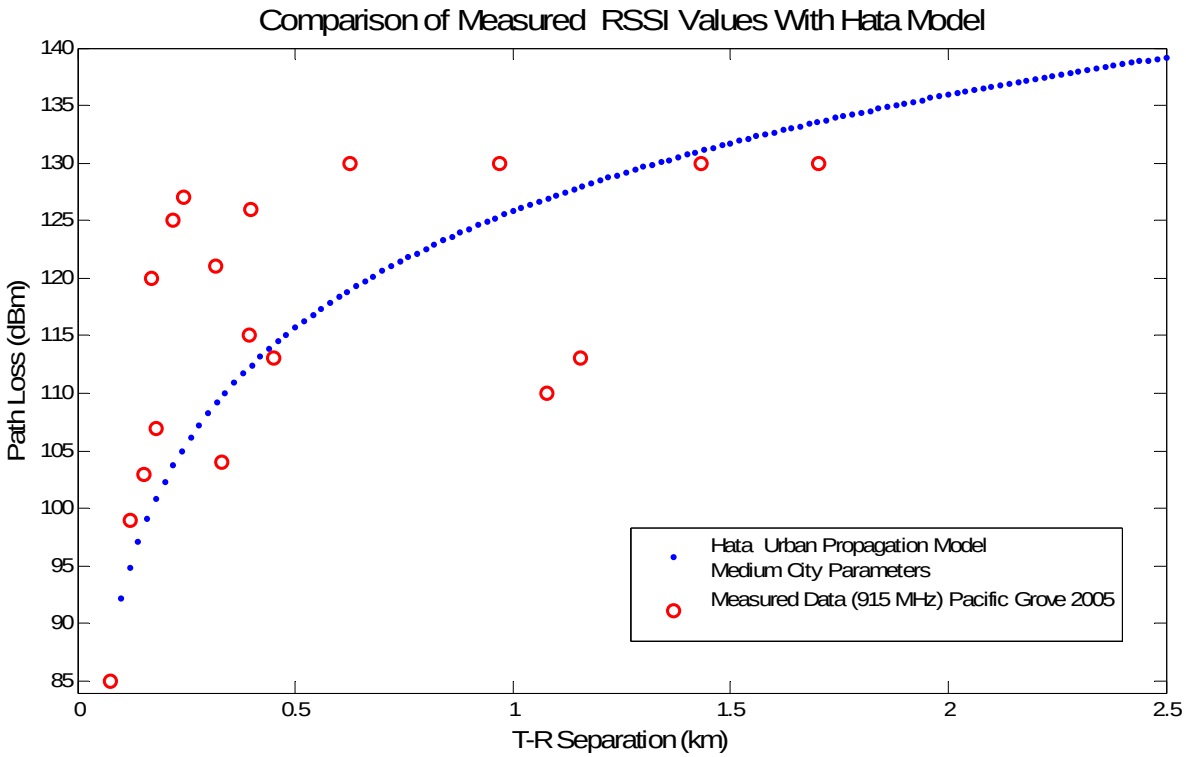

Figure 40. Comparison of measured data with the Hata Urban Propagation Model.

a. Antenna Orientation Effects in Urban Area

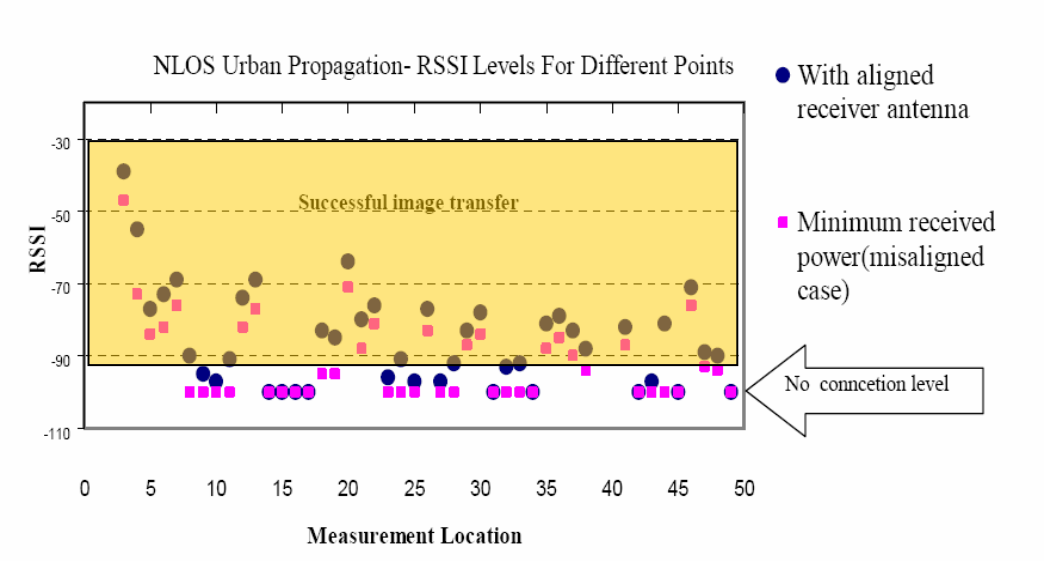

Figure 41. Antenna orientation effects on NLOS urban data link.

RSSI measurement results for the non line of sight (NLOS) urban area measurements are plotted in Figure 41. While collecting data, the worst and best RSSI levels corresponding to the misaligned and aligned cases were recorded in order to check the antenna orientation effects on NLOS communication as well. In Figure 41, dots indicate the maximum received power at the spot with aligned receiver antenna, while the squares indicate the minimum received power with disoriented receiver antenna. No connection RSSI level is marked as -94 dBm. Measurement points inside the orange zone show successful image transfer.

3. Effects of Foliage and Random Trees

Effects of random trees and foliage were studied experimentally at different sites on the NPS campus in order to simulate a forest area (Figure 42). Propagation media was classified as dense foliage and semi-dense foliage and data was collected, accordingly, to minimize the effects of the random density of trees. This classification was based on the distances between the trunks of the trees such that if there were two or more trees within the 15 meter-radius of a tree, the media was considered dense.

Figure 42. Sample foliage data measurement locations.

The effects of foliage and random trees on path loss became explicit when the foliage data was compared to free space reference data. Dense foliage was proved to increase the path loss in a very short distance. An additional 50 dBm loss was measured for dense foliage over free space loss for 300 m T-R separation (see Figure 43).

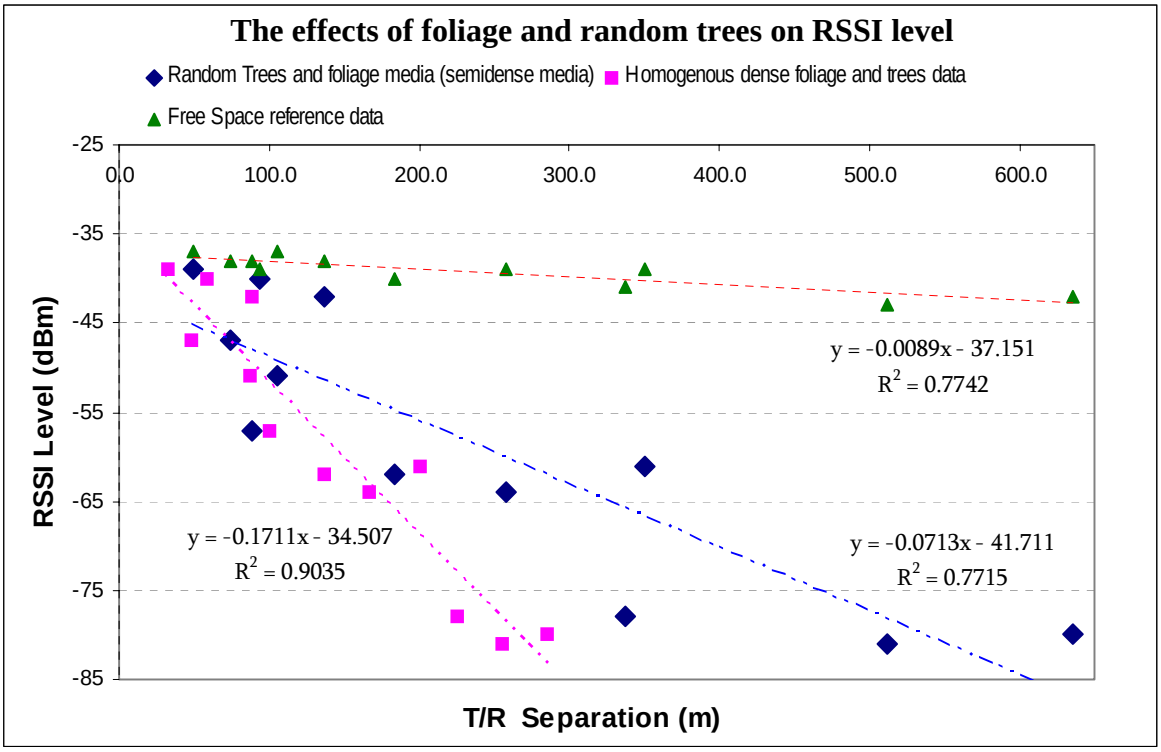

Figure 43. The effects of foliage and random trees on RSSI level.

C. INDOOR PROPAGATION MEASUREMENTS

Constituents to the path loss in an indoor propagation channel are various and complex. Propagation path of an RF signal is generally blocked by walls, floors, doors and windows. Multipath effects that are caused by reflection and diffraction contribute to the path loss at larger scales in indoor propagation. Various buildings with different structural geometries and common building materials were experimentally tested to determine the indoor capabilities of the image transfer system. Data was collected mainly in Spanagel Hall at NPS. Spanagel Hall is a six –story, strongly reinforced, rectangular structure with wide windows and glass doors. Ingersoll Hall, Watkins Hall and the Dudley Knox Library were also tested to determine outdoor to indoor propagation by measuring the received signal strengths from the transmitter antenna located on the roof of Spanagel Hall (Figure 42). Given the strong and heavy structures of these three buildings, the result was satisfactory for our system.

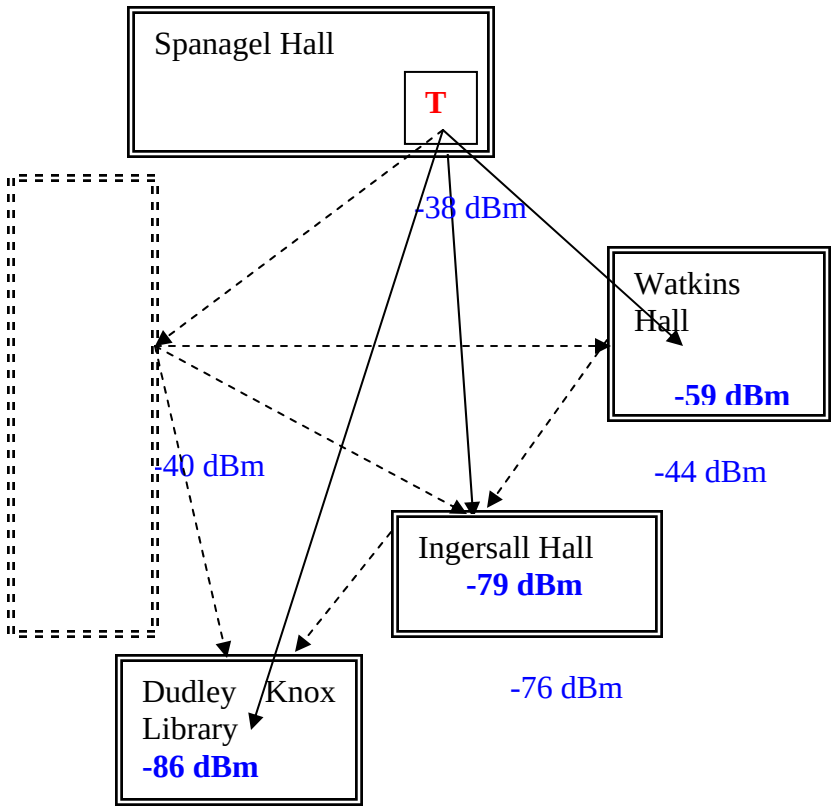

Figure 44. Outdoor to indoor measurement results at NPS campus.

1. Wall Penetration Data

Signal loss measurement results are shown through 5.8-inch single and multi-chalkboard walls in Figure 45.

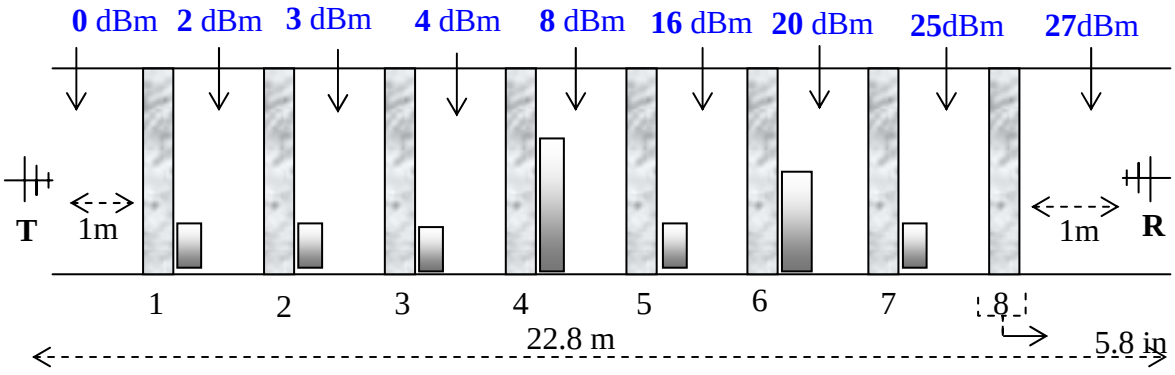

Figure 45. Path loss measurement results through eight identical walls (chalkboard). Bars inside the rooms indicate estimated furniture density.

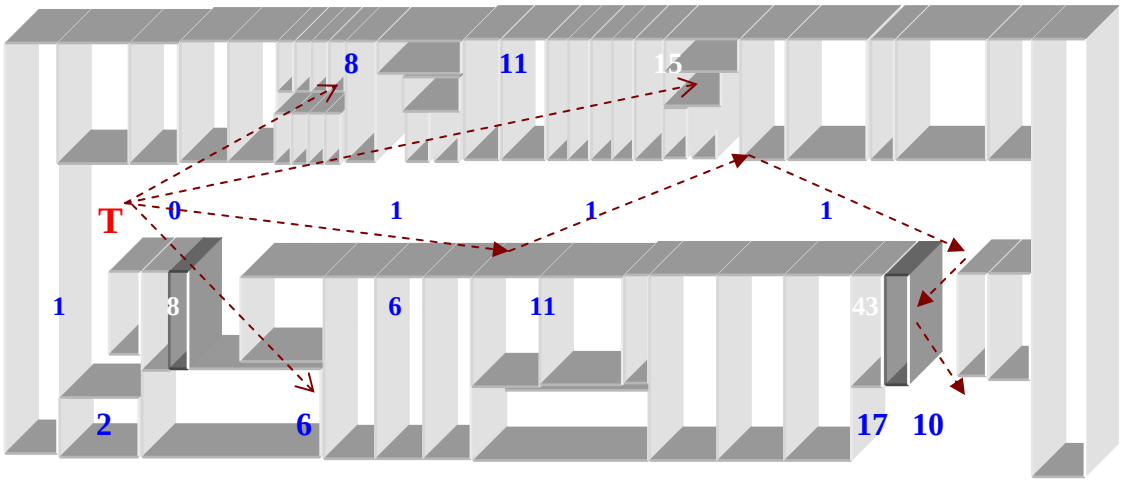

Figure 46. Propagation loss measurement results at different points in Spanagel Hall basement (numbers indicate the measured loss level at that point in dBm).

2. Floor Penetration Data

The path loss due to floor penetration depends highly on construction material and structural geometry. Previous studies [15, 16] revealed that the attenuation in signal strength between the floors of a building does not follow a linear path. In these studies the contribution of the first floor to the path loss was found to be more when compared to the loss caused by the consecutive floors in the same building. This is thought to be caused by surrounding reflected waves.

Path loss data was collected at various points on each floor of Spanagel Hall, while the transmitter antenna was located on the roof with horizontal polarization. Our measured data (represented in Figure 47) verified the above mentioned phenomenon. The largest fall of received signal power was observed on the floor which comes first on the trajectory of the propagating wave. Waves reflecting from the surrounding buildings and ground are found to cause an increase in RSSI level at the points close to the windows or doors.

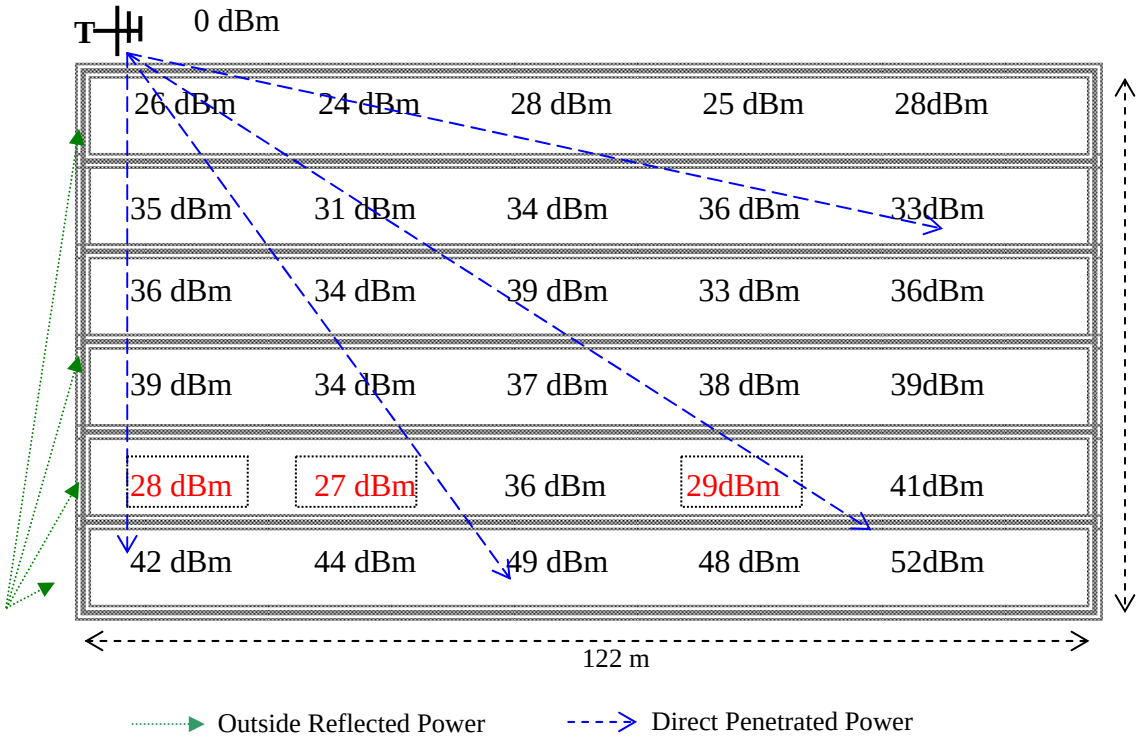

Figure 47. Spanagel Hall floor 915 MHz penetration loss levels (notice that values in the boxes coincides with the large glass doors of the building).

3. Transmission through Different Materials

The attenuation caused by different common building materials was tested experimentally in the anechoic chamber. Measurement results are displayed in Table 2. Wooden and glass doors, windows and single chalkboard walls caused minor attenuation; on the order of 1-2 dBm. Path loss for the metal containing materials were tested and found to be higher; 4-5 dBm for metal doors, 24 dBm for aluminum plate (2x2 m2) and 8-10 dBm for the reinforced cement wall reinforced with metal bars. These measurements indicate that 915 MHz is a convenient frequency for indoor propagation when compared to other higher frequencies like 2.4 GHz.

Building Components	**915 MHz Loss (dBm)**
Metal Frame Window	1-2 dBm
Glass Door (0.62 cm)	1-2 dBm
Metal Door (1 cm)	4-5 dBm
Wooden Door(1.75 in)	0-1 dBm
Single Floor	15-25 dBm
Single Wall Chalkboard (5.8 in)	2-3 dBm
Aluminum Plate (0.8 cm)	24 dBm
Brick Wall (8 in)	4-5 dBm
Reinforced Cement Wall (10.2 in)	8-10 dBm

Table 2. Path loss measurements caused by transmission through different materials.

THIS PAGE INTENTIONALLY LEFT BLANK

V. CONCLUSION

This thesis work demonstrated that a line-of-sight transmission path between the transceiver and its associated remote site(s) is highly desirable and provides the most reliable communications link for an IR image transfer system.

Possible path loss scenarios that a military data collecting system may undergo while transferring the data are studied experimentally, and the IR image system is proved to function properly at an RSSI value of as low as -90 dBm. Maximum free space communication range is measured to be 36 km when the line of sight is clear of obstacles.

The effects of objective data characteristics (i.e., file size) on image transfer performance are also investigated and found to be in the safe region for our setup.

Dense foliage and random trees are found to cause a path loss on the order of 40-50 dBm in 300 m, while sparsely populated areas have reduction effects closer to free space loss. Because of the complex geometry involved in urban propagation, path loss is difficult to estimate. Only site specific measurements will provide reliable results. The RSSI level can quickly drop to very low levels in very short ranges, rendering the radio link inoperative. Measurements around Pacific Grove yielded an effective radius of 2 km from the transmitter in which successful communication is possible.

Antenna polarization is observed to be important. Incorrect polarization caused a signal reduction of 15 dB or more during measurements. Using directional antennas improved performance to a remarkably level.

The 915 MHz frequency is tested and found to be reliable, being less vulnerable to path loss effects when compared to 2.4 GHz and higher frequencies. Interference from adjacent devices is observed to have adverse effects on file transfer performance. It has a random and site specific nature. Effects of interference are observed to decrease with use of directional antennas.

The overall performance of the image transfer system is found to be satisfactory for possible military utilization.

THIS PAGE INTENTIONALLY LEFT BLANK

APPENDIX A IR-160 CAMERA TECHNICAL SPECIFICATIONS

PARTS	PROPERTIES
Detector	160(H)x120(V) microbolometer focal plane array with CMOS ROIC
Pixel Size	50 micrometer square pixel
A/D Conversion	14 bit digitizing resolution
Cryogenic Cooling	None required
FOV	22.9 (H) x17.2 (V) with 20 mm focal length lens
IFOV	4.0 mrad with 20 mm focal length lens
Lens	Germanium 20 mm. F/0.8 focus 12” to infinity
Spectral Band	8-14 micrometer, anti-reflection coated Germanium optics
NETD	<60 mk@ 300 C
Operating Temperature	0 to 50 degrees C
Power Input	9.0 to 24.0 VDC,<5 Watts with shutter open
Frame Rate	30 Hz
Communication	RS-232
Video output	NTSC or PAL
Housing Size	4.3x3.9x4.2 in(W x H x D)
Complete Imager Weight	24.0 oz without lens

[From Ref. 1 and Ref. 8]

THIS PAGE INTENTIONALLY LEFT BLANK

APPENDIX B IR-160 CONTROL COMMANDS

CHARACTER	COMMAND	DESCRIPTION
Z	Freeze/Snapshot	Pause camera on the latest image
U	Unfreeze	Start imager running again if paused
W	White Hot	Hotter targets in the image are brighter
B	Black Hot	Hotter targets in the image are darker
<	Decrease Brightness	Makes image darker
-	Decrease Contrast	Decreases color range used for image
>	Increase Brightness	Makes image brighter
+	Increase Contrast	Increases color range used for image
I	Download Image	Transmits an 8-bit PGM file via X-Modem to the host (camera is paused during transfer)
R	Download Raw Data	Transmits raw sensor data as 16-bit signed data via X-Modem
G	Download Gain Table	Transmits the gain table as 16-bit signed data via X-Modem
/	Linear Palette	Set palette mode to linear(linear color mapping between minimum and maximum)
@	Quick Calibration	Creates a gain table to 1.0(e.g. no dead pixels, no gain correction)
$	Acquire/Download Statistics	Stores a large amount of stats in SRAM for XX frames and then sends them to the host PC via an X-Modem transfer
D	Upload DL File to Imager	Initiates X-Modem receive for a DL file, which can be gains, gamma tables, new software, etc. Reboots camera after transfer

[From Ref. 1 and Ref. 8]

THIS PAGE INTENTIONALLY LEFT BLANK

APPENDIX C MDS INET 900 TRANSCEIVER TECHNICAL SPECIFICATIONS

GENERAL

Temperature Range:	–30° C to +60° C (–22° F to 140° F)
Humidity:	95% at +40° C (104° F); non-condensing
Primary Power:	10–30 Vdc (13.8 Vdc Nominal)
External Power Supply Options:	110–120/210–220 Vac
Supply Current (typical):	(9 Watts Maximum @ 1 Watt RF Output)
Transmit:	8 watts (10.5-24 Vdc) 9 watts (24.5-30 Vdc)
Receive:	2.8 watts (10.5-24 Vdc) 3.5 watts (24.5-30 Vdc)
MTBF:	35 Years (Telcordia Method 1, Case 3)
Size (Excluding mtg. hardware):	1.4" x 6.75" x 4.5" (H x W x D) 3.56 x 17.15 x 11.43 cm
Mounting w/Optional Hardware:	• Flat surface mounting brackets
	• 19" rack (1U high)
Weight:	908 g / 2 lb
Case:	Cast Aluminum
Boot Time:	≈ 30 sec
Time Required to Associate with Access Point:	≈ 20 sec

APPROVALS/HOMOLOGATION

- FCC Part 15.247
  E5MDS-NH900
- Industry Canada RSS-210 and RSS-139
  CAN 3738A 12098
- UL/CSA Class 1, Div. 2; Groups A, B, C and D hazardous locations
- Contact factory for information on availability and governmental approvals in other countries

MANAGEMENT

- HTTP (Embedded Web server)
- Text-based menu on COM1 serial port
- Telnet
- SNMP v1/v2/v3
- MDS NETview MS™

[From Ref. 9]

Serial (2 Ports):

Signaling Standard:	EIA-232/V.24
Interface Connectors:	DB-9
Interface:	COM1: DCE / COM2: DTE
Data Rate:	1200–115,200 bps asynchronous
Data Latency:	< 10 ms typical
Byte Formats:	7 or 8-bit; even, odd, or no-parity; 1 or 2 stop bits

OPERATING MODES:

- Configurable as Access Point or Station LAN Adapter
- CSMA/CA Wireless Protocol with Collision Avoidance (802.11)

PROTOCOLS:

- IEEE 802.11 CSMA/CD (Wireless)
- IEEE 802.3 (Ethernet)
- IP/Ethernet (ICMP, UDP, TCP, ARP)
- Clear-channel mode for serial async multidrop protocols including: Modbus, DNP.3, Bisync, BSAP, DF1, TotalFlow, Poll Select

SECURITY

- Approved AP/Remotes list
- Failed login lockdown
- 900 MHz FHSS—provides inherent security from 802.11b devices
- Proprietary data framing
- 128-bit encryption
- Automatic rotating key algorithm

[From Ref. 9]

RADIO CHARACTERISTICS

GENERAL:	
Frequency Range:	902–928 MHz ISM Band
Frequency Hopping Range:	Ten user-configurable 2.5 MHz-wide zones, each containing 8 frequencies
Hop Pattern:	Based on network name
Frequency Stability:	20 ppm
TRANSMITTER:	
Power Output (at antenna connector):	0.1 to 1.0 watt (+20 dBm to +30 dBm) ±1.0 dB, *set by user*
Duty Cycle:	Continuous
Modulation Type:	Binary CPFSK
Output Impedance:	50 Ohms
Spurious:	–67 dBc
Occupied Bandwidth:	316.5 kHz
RECEIVER:	
Type:	Double conversion superheterodyne
Sensitivity:	–92 dBm @ 512 kbps < $1x10^{-6}$ BER –99 dBm @ 256 kbps < $1x10^{-6}$ BER
Intermodulation:	59 dB Minimum (EIA)
Desensitization:	70 dB
Spurious:	60 dB

[From Ref. 9]

THIS PAGE INTENTIONALLY LEFT BLANK

APPENDIX D YAGI ANTENNA SPECIFICATIONS

Scaled NBS 3 Element YAGI #2		
Freq.	0.915	GHz
Wavelength	327.87	mm
Baseline Freq	0.903	GHz
Baseline WL	332.23	mm

	Baseline (mm)	Length (w ave)	Length (mm)	Half Len (mm)	Pos (w ave)	Pos (mm)
REFLECTOR	159	0.479	156.91	78.46	0	0
Separation	66.45	0.2	65.58			
DRIVEN ELEMENT	145.4	0.438	143.49	71.75	0.2	65.58
Separation	66.45	0.2	65.58			
DIRECTOR1	143.4	0.432	141.52	70.76	0.4	131.16

Folded dipole DE	mm	inch
Fold Sep	12	0.472
Full Arc Circle	37.7	1.484
MidArc - MidArc	150.34	5.919
Drive Pt. Gap	3	0.118
Tot Rod Len	297.69	11.72
Rod End to MidArc	73.67	2.9

[From Ref. 1 and Ref. 17]

THIS PAGE INTENTIONALLY LEFT BLANK

APPENDIX E CONVERSION TABLE

dBm	V	Po
+53	100.0	200W
+50	70.7	100W
+49	64.0	80W
+48	58.0	64W
+47	50.0	50W
+46	44.5	40W
+45	40.0	32W
+44	32.5	25W
+43	32.0	20W
+42	28.0	16W
+41	26.2	12.5W
+40	22.5	10W
+39	20.0	8W
+38	18.0	6.4W
+37	16.0	5W
+36	14.1	4W
+35	12.5	3.2W
+34	11.5	2.5W
+33	10.0	2W
+32	9.0	1.6W
+31	8.0	1.25W
+30	7.10	1.0W
+29	6.40	800mW
+28	5.80	640mW
+27	5.00	500mW
+26	4.45	400mW
+25	4.00	320mW
+24	3.55	250mW
+23	3.20	200mW
+22	2.80	160mW
+21	2.52	125mW
+20	2.25	100mW
+19	2.00	80mW
+18	1.80	64mW
+17	1.60	50mW
+16	1.41	40mW
+15	1.25	32mW
+14	1.15	25mW
+13	1.00	20mW
+12	.90	16mW
+11	.80	12.5mW
+10	.71	10mW
+9	.64	8mW
+8	.58	6.4mW
+7	.500	5mW
+6	.445	4mW
+5	.400	3.2mW
+4	.355	2.5mW
+3	.320	2.0mW
+2	.280	1.6mW
+1	.252	1.25mW

dBm	V	Po
0	.225	1.0mW
-1	.200	.80mW
-2	.180	.64mW
-3	.160	.50mW
-4	.141	.40mW
-5	.125	.32mW
-6	.115	.25mW
-7	.100	.20mW
-8	.090	.16mW
-9	.080	.125mW
-10	.071	.10mW
-11	.064	
-12	.058	
-13	.050	
-14	.045	
-15	.040	
-16	.0355	

dBm	mV	Po
-17	31.5	
-18	28.5	
-19	25.1	
-20	22.5	.01mW
-21	20.0	
-22	17.9	
-23	15.9	
-24	14.1	
-25	12.8	
-26	11.5	
-27	10.0	
-28	8.9	
-29	8.0	
-30	7.1	.001mW
-31	6.25	
-32	5.8	
-33	5.0	
-34	4.5	
-35	4.0	
-36	3.5	
-37	3.2	
-38	2.85	
-39	2.5	
-40	2.25	.1µW
-41	2.0	
-42	1.8	
-43	1.6	
-44	1.4	
-45	1.25	
-46	1.18	
-47	1.00	
-48	0.90	

dBm	mV	Po
-49	0.80	
-50	0.71	.01µW
-51	0.64	
-52	0.57	
-53	0.50	
-54	0.45	
-55	0.40	
-56	0.351	
-57	0.32	
-58	0.286	
-59	0.251	
-60	0.225	.001µW
-61	0.200	
-62	0.180	
-63	0.160	
-64	0.141	

dBm	µV	Po
-65	128	
-66	115	
-67	100	
-68	90	
-69	80	
-70	71	.1nW
-71	65	
-72	58	
-73	50	
-74	45	
-75	40	
-76	35	
-77	32	
-78	29	
-79	25	
-80	22.5	.01nW
-81	20.0	
-82	18.0	
-83	16.0	
-84	11.1	
-85	12.9	
-86	11.5	
-87	10.0	
-88	9.0	
-89	8.0	
-90	7.1	.001nW
-91	6.1	
-92	5.75	
-93	5.0	
-94	4.5	
-95	4.0	
-96	3.51	
-97	3.2	

dBm	µV	Po
-98	2.9	
-99	2.51	
-100	2.25	.1pW
-101	2.0	
-102	1.8	
-103	1.6	
-104	1.41	
-105	1.27	
-106	1.18	

dBm	nV	Po
-107	1000	
-108	900	
-109	800	
-110	710	.01pW
-111	640	
-112	580	
-113	500	
-114	450	
-115	400	
-116	355	
-117	325	
-118	285	
-119	251	
-120	225	.001pW
-121	200	
-122	180	
-123	160	
-124	141	
-125	128	
-126	117	
-127	100	
-128	90	
-129	80	.1*f*W
-130	71	
-131	61	
-132	58	
-133	50	
-134	45	
-135	40	
-136	35	
-137	33	
-138	29	
-139	25	
-140	23	.01*f*W

[From Ref. 9]

THIS PAGE INTENTIONALLY LEFT BLANK

LIST OF REFERENCES

[1] Ata, A., "Wireless IR Image Transfer System for an Autonomous Vehicle," Master's Thesis, Naval Postgraduate School, December 2003.

[2] Rappaport, T.S., Wireless Communications: Principles and Practice, New Jersey: Prentice Hall Publications, 1996.

[3] Gibson, T.B., "Propagation Loss Study and Antenna Design for the Micro-Remotely Powered Vehicle (MRPV)," Master's Thesis, Naval Postgraduate School, September 1995.

[4] Griffiths, D.J., Introduction to Electrodynamics, Third Edition, New Jersey: Prentice Hall Publications, 1999.

[5] Anderson, R. H., Fixed Broadband Wireless System Design, New Jersey: John Wiley & Sons, Inc., 2003.

[6] Miller, L.E., "Propagation Model Sensitivity Study," Contract Report, J.S. Lee Associates, Inc., July 1992, (DTIC A.N. AD-B166479).

[7] Epstein, J. and Peterson, D.W., "An Experimental Study of Wave Propagation at 850 Mc," Proceedings of Proceedings of the Institute of Radio Engineers , Vol. 41, pp. 595-611, May 1953.

[8] Infrared Solutions, Inc., "IR-160 Thermal Imager," October 2003, (http://www.infraredsolutions.com), 01/17/2005.

[9] Microwave Data Systems, Inc., "MDS iNET 900 User's Guide," August 2003.

[10] Bertoni, Henry L., "Radio Propagation for Modern Wireless Systems," Upper Saddle River, New Jersey: Prentice Hall PTR, 2000.

[11] Jenn, D., "Basic Antenna Parameters and Wire Antennas," Lecture Notes Volume II, Department of Electrical and Computer Engineering, Naval Postgraduate School.

[12] Hata, M., “Empirical Formula for Propagation Loss in Land Mobile Radio Service,” IEEE Transactions on Vehicular Technology, Vol. VT-29, pp. 317-325, 1980.

[13] Jenn, D., “Overview of EM Wave Propagation,” Lecture Notes, Department of Electrical and Computer Engineering, Naval Postgraduate School.

[14] Lecours, M., Chouina Signard, I.Y., Delisle, G.Y. and Roy, J., “A Statistical Model for Received Signal Envelope in a Mobile Radio Channel,” IEEE Transactions on Vehicular Technology, Vol. VT-37, pp. 204-212, 1988.

[15] Honcharenko, W., Bertoni, H.L. and Dailing, J., “Mechanisms Governing Propagation between Floors in Buildings,” IEEE Transactions on Antennas and Propagation, Vol. 41, No. 6, pp. 787-790, June 1993.

[16] Andersen, J.B., Rappaport, T.S. and Yoshida, S., “Propagation Measurements and Models for Wireless Communications Channels,” IEEE Communications, 1995.

[17] Yagi antenna design by Thomas Hoffler, Naval Postgraduate School, 2003.

[18] Struzak, R., “Basic Antenna Theory”, Presentation, The Abdus Salam International Centre for Theoretical Physics ICTP, Trieste (Italy), 2005.

(http://wireless.ictp.it/school_2005/lectures/struzak/Anten_theor_basics.pdf), 05/06/2005.

INITIAL DISTRIBUTION LIST

1. Defense Technical Information Center
   Ft. Belvoir, Virginia

2. Dudley Knox Library
   Naval Postgraduate School
   Monterey, California

3. Chairman (Code PH)
   Department of Physics
   Naval Postgraduate School
   Monterey, California

4. Richard M. Harkins
   Naval Postgraduate School
   Monterey, California

5. Gamani Karunasiri
   Naval Postgraduate School
   Monterey, California

6. Kara Harp Okulu Komutanligi
   Ankara, Turkey

7. Oktay Felekoglu
   Kara Harp Okulu
   Ogr. A. 2nci Tb.8nci Bl.
   Ankara, Turkey

8. Huseyin Felekoglu
   Cakmak Mah. Baraj Sok.
   Cakmak Ilkogr. Okulu
   Umraniye, 81260
   Istanbul, Turkey